NASA CONTRACTOR REPORT

NASA CR-2432

NASA CR-2432

ACOUSTIC RADAR INVESTIGATIONS OF BOUNDARY LAYER PHENOMENA

by Jacky R. Marks

Prepared by
UNIVERSITY OF OKLAHOMA
Norman, Okla. 73069
for George C. Marshall Space Flight Center

NATIONAL AERONAUTICS AND SPACE ADMINISTRATION • WASHINGTON, D. C. • MAY 1974

TECHNICAL REPORT STANDARD TITLE PAGE

1. REPORT NO.	2. GOVERNMENT ACCESSION NO.	3. RECIPIENT'S CATALOG NO.
CR-2432		

4. TITLE AND SUBTITLE	5. REPORT DATE
Acoustic Radar Investigations of Boundary Layer Phenomena	May 1974
	6. PERFORMING ORGANIZATION CODE M128
7. AUTHOR(S) Jacky R. Marks	8. PERFORMING ORGANIZATION REPORT #
9. PERFORMING ORGANIZATION NAME AND ADDRESS University of Oklahoma Norman, Oklahoma 73069	10. WORK UNIT NO.
	11. CONTRACT OR GRANT NO. NAS8-28659
12. SPONSORING AGENCY NAME AND ADDRESS National Aeronautics and Space Administration Washington, D.C. 20546	13. TYPE OF REPORT & PERIOD COVERED Contractor
	14. SPONSORING AGENCY CODE

15. SUPPLEMENTARY NOTES

Prepared under the technical monitorship of the Aerospace Environment Division, Aero-Astrodynamics Laboratory, NASA-Marshall Space Flight Center.

16. ABSTRACT

A comparison is made between acoustic radar echoes and conventional meteorological data obtained from the WKY tower, for the purpose of better understanding the relationships between acoustic radar echoes and boundary layer processes.

Two thunderstorm outflow cases are presented and compared to both acoustic radar data and Charba's gust front model. It is found that the acoustic radar echoes reveal the boundary between warm and cold air and other areas of mixing and strong thermal gradient quite well. The thunderstorm outflow of 27 June 1972 is found to compare well in most respects to Charba's gust front model. The major difference is the complete separation of the head from the main body of cold air, probably caused by erosion of the area behind the head by mixing with the ambient air. The second case is found not to compare as well, probably due to the weakness of the storm.

Two cases of nocturnal inversions caused by advection of warmer air aloft are presented. It is found that areas of turbulent mixing or strong thermal gradient can be identified quite easily in the acoustic radar record. Possible mechanisms for the formation and dissolution of these inversions are discussed, and related to the synoptic pattern.

It is concluded that the qualitative data afforded by acoustic radar echo patterns can be quite valuable in the study of the boundary layer.

17. KEY WORDS	18. DISTRIBUTION STATEMENT
Acoustic Radar Nocturnal Inversions Doppler	CAT. 20

19. SECURITY CLASSIF. (of this report)	20. SECURITY CLASSIF. (of this page)	21. NO. OF PAGES	22. PRICE
Unclassified	Unclassified	65	$3.75

ACKNOWLEDGMENTS

The author wishes to thank the Air Force Institute of Technology for providing the scholarship which permitted the study leading to the accomplishment of this thesis. Also sincere appreciation is expressed to Dr. Rex L. Inman under whose guidance this research was done. His knowledge and assistance were essential in the completion of this study. Sincere gratitude is expressed to Captain E. H. Kelly for his stimulating discussions and help in preparing the illustrations. Expression of thanks is extended to other members of the staff for their review of the thesis. Appreciation is also extended to the personnel of the National Severe Storms Laboratory for the use of their facilities and for providing timely and accurate data.

This research was done in connection with graduate study at the University of Oklahoma. This research was partially supported by the Atmospheric Sciences Section, National Science Foundation, NSF Grant GA-35403 and by George C. Marshall Space Flight Center, contract NAS8-28659.

TABLE OF CONTENTS

LIST OF TABLES

LIST OF ILLUSTRATIONS

LIST OF SYMBOLS

A	antenna collecting area (m^2)
C_T	the temperature structure constant ($K\ cm^{-1/3}$)
c	velocity of sound ($m\ sec^{-1}$)
D_T	the temperature structure function (K^2)
L	an attenuation factor
P	transmitted acoustic power (w)
P_r	received acoustic power (w)
R	the range (m)
R_i	the gradient Richardson number
T	temperature (K)
λ	transmitted wave length (cm)
σ	scattered power per unit volume per unit incident flux per unit solid angle in the backscatter direction
τ	transmitted pulse length (sec)

ACOUSTIC RADAR INVESTIGATIONS OF BOUNDARY LAYER PHENOMENA

CHAPTER I

INTRODUCTION

One of the great challenges facing meteorology today is that of understanding the planetary boundary layer. Surface friction, surface heating and other effects make the study of the boundary layer exceedingly more complex than that of the free atmosphere. Understanding of the boundary layer and the role it plays in local processes such as severe storms and in larger scale processes must come before significant improvement can be made in forecasting schemes in all scales of motion. Severe weather forecasting has been especially affected by lack of knowledge of the boundary layer.

In recent years significant advances have been made in understanding the surface friction layer, but such has not been the case for the "Ekman layer". The lack of advance in understanding of this layer has largely been the result of the difficulty in obtaining data. Most of the data obtained on

the "Ekman layer" thus far has come from balloon-borne packages, aircraft, and the few instrumented towers available. Each of these methods is either expensive, or will not provide the quality and accuracy of data needed, or both. Further, all these methods disturb the field in which the measurement is made, at least to some extent. For these reasons attention has turned in recent years to remote sensing of the planetary boundary layer.

One of the most promising remote sensing instruments developed in recent years is the acoustic radar. The acoustic radar is highly sensitive to fluctuations in both temperature and velocity, much more so than either electromagnetic radar or lidar. Further enhancing its attractiveness in boundary layer applications is its low cost of construction and operation.

The history of the study of acoustic backscattering has, like most scientific developments been one of interest followed by periods of relative inactivity. Tyndall (1875), while studying the propagation of sound from a large fog horn, detected acoustic backscatter from thermal and wind structure in the atmosphere and attributed it to "acoustic clouds" or to the "flocculent" nature of the atmosphere. By using a sensitive flame detector, he was able to show that heated air could

attenuate the direct propagation of sound and lead to back-scattering.

The next significant event in acoustic echo-sounding did not occur until 1944 when Gilman et al. (1946) used acoustic backscatter to study low-level temperature inversions which were causing radio-wave fading. They discovered that the backscattered signal revealed an amazing amount of atmospheric structure beneath these inversions. The intensity of the acoustic echoes they received was unexpectedly high, much higher than the theoretical predictions for the reflection of sound from strong temperature gradients. The conclusion they reached was that the received echoes were due not only to strong temperature gradients but also to turbulent temperature fluctuations. Moreover, they concluded that turbulent temperature fluctuations were the primary scatterer of the acoustic signal.

Little further development occurred until McAllister (1968) set up an acoustic sounding test site in Australia in 1967. The purpose of the experiments was to develop a means to monitor the lower atmosphere for the purpose of detecting conditions conducive to radio wave fading. The results obtained, however, had a much wider application. McAllister found that acoustic energy could be used to probe the atmosphere and that the

detected backscattered energy could be used to obtain a visual record of turbulent temperature fluctuations as a continuous function of height and time. Later McAllister et al. (1969) presented a more detailed report of this experiment in which he described observations of various meteorological phenomena such as thermal plumes, breaking waves and radiation inversions. The acoustic radar data was compared to conventional meteorological data received from an instrumented 75 m tower. McAllister's experiments confirmed the conclusions of Gilman et al. (1946) that backscattered acoustic energy is primarily due to turbulent temperature fluctuations.

Little (1969) reviewed the potential usefulness of acoustic probing of the atmosphere. He pointed out that acoustic methods should prove especially valuable in the study of the boundary layer. He further suggested that acoustic sounding methods could be developed to monitor temperature inversions, mechanical turbulence, temperature fluctuations, and the vertical profiles of wind speed, wind direction and humidity.

Beran et al. (1971) used the Doppler shift in frequency of the received acoustic signal to determine vertical velocities in the boundary layer. They calculated detailed vertical velocity patterns within individual thermals and within an inversion at a time when breaking gravity waves were present, accurate

to about $\pm$ 0.2 m sec^{-1}. They also pointed out the utility of the acoustic Doppler approach in the study of convection and wave phenomena in the atmosphere.

An acoustic radar was constructed and placed in operation at the University of Oklahoma in 1971. Preliminary results were reported by Cronenwett et al. (1972). Results of preliminary studies led to modification and improvement of the equipment, and since June of 1971 the acoustic radar has been in operation at a site near the meteorologically instrumented WKY television tower. The WKY tower is located about 6 n mi north of Oklahoma City, Oklahoma, in gently rolling terrain. The acoustic radar is situated approximately 450 m from the tower.

The tower data acquisition system has been described by Carter (1970). The tower is instrumented at seven levels (23, 45, 90, 177, 266, 355, and 444 m). Temperatures, wind speeds, and wind directions are recorded at all seven levels. Vertical velocities and wet-bulb temperatures are recorded at three levels (23, 177, and 444 m).

The original purpose of this research was to determine vertical velocities in the boundary layer, from the Doppler shift in frequency of the returned acoustic signal. The transmitted and returned signals were recorded on tape, digitized and processed by computer. The received signal was digitized

in 512 word segments with a sampling time of 110 μ sec and a fast Fourier transform was performed on the digitized data to obtain the received signal spectrum. The received frequency was then determined by inspection of the spectrum. It was found that the received frequency determined by this method did not meet the resolution requirements demanded for computation of vertical velocities. The resolution of a fast Fourier transform depends upon the number of data points available. The 512 word sample did not provide enough data points for proper frequency resolution. Since vertical resolution would have suffered if the number of words in the sample were increased, it was decided that the fast Fourier transform method was not suitable.

It was then decided to determine the received frequency by counting the zero crossings in the digitized data. However, after several weeks of trying different filtering and processing techniques, it was decided that this approach was also unsuitable due to noise in the signal and difficulty in processing in areas of weak returns. Work is now underway to provide on-equipment processing of vertical velocities.

Following the failure to obtain reliable estimations of vertical velocities, attention was focused on interpretation of the acoustic facsimile records and their relationships with

on-going boundary layer processes. Major emphasis has been placed on the study of cold air outflow from thunderstorms and the formation and dissolution of nocturnal inversions. Results are discussed as case studies, relating the synoptic situation, data obtained from the tower, and the acoustic radar data. Conventional teletype and facsimile data were used for determination of the synoptic situation and to augment on-site data.

Previous studies have greatly advanced knowledge in the area of pattern recognition and interpretation of acoustic echoes. However, previous studies have not had the advantage of operating in conjunction with a meteorologically instrumented tower as tall (450 m) as the WKY tower. The main purpose of this research has been to interpret the acoustic record and determine the relationships existing between acoustic echo patterns and boundary layer processes. A further purpose has been to further confirm, as theory predicts, that acoustic backscatter results only from interaction of the acoustic signal with turbulent fluctuations of temperature and strong thermal gradients. A third purpose has been to increase knowledge of the structure of gust fronts and nocturnal inversions.

CHAPTER II

ACOUSTIC RADAR THEORY AND OPERATION

Acoustic energy in general interacts much more strongly with the atmosphere than does electromagnetic energy. The strong interaction results because the atmosphere is the transmitting vehicle for acoustic waves, whereas it is only a perturbation for the propagation of electromagnetic waves, such as those produced by conventional radar or lidar. Because of this strong interaction acoustic echo-sounding equipment can be built much more cheaply and simply than other radar devices relying upon electromagnetic propagation.

Transmission of acoustic energy into the atmosphere may result in scattering, reflection, or absorption. Reflection occurs when the acoustic energy encounters sharp vertical gradients in the mean air temperature. Scattering is caused by turbulent fluctuations of temperature and wind velocity, and by particulates. Variations in water vapor pressure also affect acoustic energy transmitted into the atmosphere. However, calculations made by McAllister et al. (1969) indicate

that the effects of water vapor upon transmission are below the threshold of detectability of present receivers.

The scattering of acoustic radiation in dry air has been quantitatively treated by Kallistratova (1961). Several important conclusions can be drawn from the equations of Kallistratova and those of Monin (1962): (1) Most of the acoustic energy is scattered in the forward direction. (2) No acoustic energy is scattered at an angle of 90° with respect to the direction of propagation, since sound is a longitudinal vibration. (3) Acoustic power varies weakly with wave length. (4) Acoustic power is scattered by wind fluctuations and temperature fluctuations. (5) Wind fluctuations produce no scatter in the backward direction (180°); all backscattered energy is the result of temperature fluctuations. The latter point is very important for our purposes, since all observations reported in this research were obtained by operating the acoustic radar in the monostatic mode.

The backscattering acoustic radar equation as given by McAllister et al. (1969) for isotropic homogeneous turbulence is

$$P_r = 0.5\ (Pc\tau AL\sigma)\ R^{-2}, \qquad (1)$$

where P_r is the received acoustic power (w), P is the transmitted acoustic power (w), c is the velocity of sound (m sec^{-1}), τ is

the transmitted pulse length (sec), A is the collecting area of the antenna (m^2), L is an attenuation factor which accounts for transducer efficiencies, atmospheric attenuation, and antenna efficiency, R is the range (m), and σ is the scattered power per unit volume per unit incident flux per unit solid angle in the backscatter direction. The equation for σ is given by McAllister (1969) as

$$\sigma = 0.008 \ (C_T^2 \lambda^{-1/3}) \ T^{-2}, \qquad (2)$$

where λ is the transmitted wave length (cm), T is the temperature (K), and C_T is a measure of the temperature fluctuation intensity ($K \ Cm^{-1/3}$). The value of C_T can be calculated from the structure function of the temperature field given by

$$D_T = \overline{[T \ (x) - T \ (x+r)]^2} = C_T^2 r^{2/3}, \qquad (3)$$

where T (x) and T (x+r) are instantaneous temperatures at the points x and x+r in the $\vec{r}$ direction. Therefore C_T^2 can be interpreted as the mean square of the temperature difference between two points in space separated by a unit distance. The above equations account only for that portion of the acoustic energy which is backscattered as a result of turbulent fluctuations of temperature. Backscattering due to specular reflection of acoustic energy in regions of sharp temperature gradients is not included.

The upper limit on the range of an acoustic radar is a function of the speed of sound and the pulse repetition frequency of the radar. However other factors can reduce the effective range to below this value. Some of these factors are atmospheric absorption, receiver limitations, and noise.

Atmospheric absorption decreases the effective range by decreasing the amount of power available for backscattering. Absorption increases as the transmitted frequency increases and as the relative humidity of the air increases. Absorption decreases with increasing temperature.

Noise not only limits the effective range but can, in extreme cases, render the acoustic radar totally useless by obscuring all valid echoes. Attenuation caused by absorption and by loss of that part of the transmitted signal which was backscattered before reaching the level in question, results in a decrease of received power as the range of scatterers increases. Since received power decreases as the range of scatterers increases, obscuration of the received signal by noise becomes more critical as range increases. The most important sources of noise are raindrops which strike the antenna and wind. High winds or heavy rain can produce noise sufficient to obscure even the strongest echoes. Environmental noise is less important in most cases, since it may be minimized by judicious site selection.

The acoustic radar used in this research is a pulsed radar which sends out a brief burst of acoustic energy. Backscattered or reflected energy is then detected by the receiver, amplified and displayed or recorded. The functional operation of the units composing the radar are not radically different from those encountered in conventional electromagnetic pulsed radars, since the basic principles underlying both are the same. However, due to the different types of energy involved, acoustic radar circuits can be constructed much more simply than those of conventional radar. A functional block diagram of the acoustic radar is shown in Fig. 1 and equipment parameters are listed in Table 1.

As shown in Fig. 1 the facsimile recorder provides the synchronization for the start of the transmission cycle. When the facsimile recorder begins its trace, a synchronizing pulse is sent to the tone burst generator. This pulse allows the tone burst generator to gate a short burst of audio signal at the transmitting frequency from the audio oscillator through a filter to the power amplifier. The amplified audio pulse is coupled by a line transformer to the transmission line which carries the pulse to the transducer site, where another line transformer couples the signal through the transmit-receive switch (TR) to the transducer. The transducer converts the

signal to vertically-directed sound. The TR switch provides a very important function. Since the transducer is used both as a transmitter and as a receiving antenna, some means must be provided to keep the high-power transmitted pulse from entering the receiver section of the radar. The TR switch provides this means, disconnecting the receiver system from the transducer while transmission is underway.

A short time after transmission has begun the sequence timer, which had been activated by a pulse from the tone burst generator at the beginning of transmission, resets the TR switch. Since signal amplitude decreases as range increases, some method must be provided to increase the receiver gain as a function of range, so that equal amplitude disturbances at differing ranges will be depicted as such. The sequence timer provides this means in the form of a voltage which increases linearly with time during each cycle (Ramp). The received signal is multiplied by the Ramp to achieve the desired gain.

Acoustic returns are converted to a voltage by the transducer and conveyed through the TR switch to the preamplifier which provides initial amplification. The received signal then passes through the receiver and the amplifier to the multiplier, where it is combined with the Ramp. The signal then passes through the recorder driver to the facsimile recorder, ending the cycle.

CHAPTER III

COLD OUTFLOW FROM THUNDERSTORMS

Case I

Charba (1972), in his study of the intense gust front leading the squall line of 31 May 1969, advanced the theory that a gust front is essentially a gravity current caused by outflow of cold air from downdrafts in areas of severe thunderstorm activity. Essential elements of Charba's gust front model are shown in Figs. 2 and 3 (Charba, 1972). The wind-shift line is caused by a pressure jump propagating on an inversion ahead of the thunderstorm activity; no change in air mass accompanies this line. The gust surge is an intense sudden increase in the speed and gustiness of the wind and is coupled with strong upward motion. The density surge line, which marks the interface between ambient air and the elevated head of the cold air mass, follows the gust surge. The density surge line marks the leading edge of the elevated pressure head.[1] Surface friction causes retardation in the lower

[1]The term head, used here as an analogy to heads in laboratory gravity currents describes the area at the front of the cold air mass where the depth of the cold air is greater than at points upstream (Fig. 3).

portions of the head, which results in the formation of a protruding nose and an area of mixing below this nose. Vertical motion behind the head is downward. A broad thermal maximum exists in this region, caused by adiabatic heating and mixing of the cold air with the ambient air from above. Following the thermal maximum, a wind speed minimum occurs coincident with a maximum of wind gustiness. After this minimum a secondary wind shift and speed maximum precede the arrival of an even colder air mass.

Although the situation on 27 June 1972 was substantially different from that on which Charba built his model, comparison can still be fruitful if the following considerations are kept in mind: (1) The cold outflow on 27 June 1972 resulted from a single intense thunderstorm and not from a squall line. (2) The observation site was not in the direct path of the storm. The center of the storm passed approximately 6 n mi to the south of the site on its path from west to east. (3) Only point observations were made. Despite these differences, there was substantial agreement with Charba's model. The following discussion is intended not only to substantiate these points, but also to show the capabilities and limitations of the acoustic radar in thunderstorm outflow situations.

The synoptic situation in central Oklahoma preceding the thunderstorm activity of 27 June 1972 is shown in Figs. 4 and 5. An elongated surface low was centered over west central Oklahoma, with its major axis oriented southwest-northeast. An 850-mb trough was oriented north-south from the central Dakotas through the Texas Panhandle to the Big Bend area. A weak, quasi-stationary front lay in the vicinity of the Oklahoma City area. Dry air was present at both the surface and at 700 mb in western Oklahoma and the Texas Panhandle. A weak trough at 700 mb was present over the Texas Panhandle (Fig. 5). The lifted index at Oklahoma City at 0600 CST was -8.

At 1510 CST, a rapidly building isolated thunderstorm west of Oklahoma City, moving eastward, was detected on the WSR-57 weather radar at the National Severe Storms Laboratory in Norman. At 1540 CST the storm entered the extreme western edge of Oklahoma City. Baseball size hail was reported in the City. Tinker Air Force Base, on the eastern edge of the City, later reported winds in excess of 70 mph from the same storm. At 1625 CST the center of the storm, as determined by radar, lay directly south of the WKY tower and acoustic radar site, which is situated about 6 n mi north of downtown Oklahoma City. Precipitation at the radar site was limited to a few sprinkles.

Prior to the wind shift, which began at 1625 (Fig. 8d), winds were uniform easterly at all levels of the tower. During the wind shift, winds in the lower levels switched to the southwest. A distinct wind speed minimum (Fig. 8c) occurred coincident with the windshift at all levels. This wind speed minimum has been described by Charba (1972) as a typical gust front feature. No change in air mass properties occurred across the wind shift. There was essentially no change in either temperature (Fig. 8b) or wet bulb temperature across the wind shift. A sharp pressure rise was measured coincident with the wind shift (Fig. 7). Pressure continued to rise after the wind shift so that no distinct leveling off of pressure occurred between the wind shift and the arrival of the gust front. Charba associated the wind shift not to the gust front, but to a pressure jump propagating ahead of the gust front. In the case being discussed the gust front follows the wind shift so closely that one might question such a separation of the origin of the wind shift and the gust front. However, it should be noted, as explained below that a surface pressure rise of 1.1 mb cannot possibly be explained as due to influx of colder air. The maximum temperature decrease across the gust front was 1.3C; this occurred at 266 m. Furthermore, the temperature decrease of only 0.3C at the top of the tower

indicates that the cold air did not extend much above this level. The surface pressure dropped 0.3 mb after passage of the initial surge of cold air. Thus, it seems reasonable to attribute 0.3 mb of the initial 1.1 mb rise to the effect of the cold air. The remaining 0.8 mb rise was probably due to a weak hydraulic jump. The calculated depth of the cold air associated with a 0.3 mb pressure rise and the temperature drop described above is approximately 800 m. A surface pressure rise of 0.2 mb (Fig. 7) accompanied the arrival of the main mass of cold air at 1638 (Fig. 8b).

The leading edge of the gust front arrived at 1629, shortly after the wind shift. Maximum winds in the gust surge were 11 m sec^{-1} at 100 m (Fig. 8c). The axis of maximum wind speeds is significantly retarded near the ground, as is the axis of minimum temperature (Fig. 8b). Rapidly fluctuating wind speeds below 50 m prior to the arrival of the gust surge at this level are indicative of turbulent mixing below this level. The protruding nose can be seen in both the temperature and the wind analyses. Temperatures began dropping at the 90- and 177-m levels approximately one min before dropping at other levels. A broad zone of upward vertical motion occurred in advance of the head, with maximum vertical velocities of 1.5 m sec^{-1} at 444 m. Downward vertical velocities behind the head were even stronger, with a maximum of -3 m sec^{-1} at the 444 m level.

These strong downward currents behind the head caused the formation of a broad thermal maximum (Fig. 8b), with maximum temperatures near the surface exceeding the ambient air temperatures. Apparently there was insufficient inflow of cold air from the thunderstorm to counteract the effects of adiabatic heating and mixing with the ambient air. As a result the head was completely separated from the cold air upstream.

Acoustic radar echoes from the cold air in the head during the period 1630 to 1635 CST (Fig. 8a) were weak because of the small temperature differences between the head and the ambient air. Stronger echoes below 200 m are indicative of the stronger mixing near the surface. The dark pin-point like returns from 200 to 700 m are suspected to be acoustic reflections from raindrops which evaporated before they reached the ground (Little, 1972), or from particulates. Possibly they could be caused by dust particles swept up into the circulation of the head, although no significant dust concentrations were visible when the head passed the site. Weak or no returns were received from 1635 to 1638 CST.

A wind speed minimum (Fig. 8c) preceded the secondary wind shift (Fig. 8d) and increase in wind speeds which marked the arrival of the second, colder mass of air. As indicated previously, the surface pressure rose 0.2 mb at this point (Fig. 7). Tower data indicates that this air mass was largely

confined below 450 m. Maximum height of strong acoustic radar returns (Fig. 8a) was 474 m with very weak echoes extending to 550 m. This air mass was also retarded near the ground during the period 1638 to 1643 CST (Fig. 8b); gustiness of the wind below 50 m during this period also indicates turbulent mixing in this layer. A secondary elevated head is also evident in the temperature analysis, with a protruding nose extending from 50 to 180 m. Maximum wind speeds of 6 m sec^{-1} occurred within this secondary head (Fig. 8c), compared with 11 m sec^{-1} observed in the primary gust surge. Maximum upward vertical velocities of 1.7 m sec^{-1} occurred immediately preceding the secondary head at 444 m. A weak zone of downward motion occurred behind the head. The situation at 177 m was substantially different, however. Upward vertical velocities preceding the head were weak but vertical velocities of -1.3 m sec^{-1} occurred in the region immediately following the head. Vertical velocities of 1.3 m sec^{-1} were observed at 177 m immediately preceding the temporary increase in the depth of the cold air mass at 1649. Afterward vertical motion was downward at all levels with a maximum of -1.9 m sec^{-1} at 444 m. Vertical velocities in the core of the cold air mass were small.

The acoustic facsimile record (Fig. 8a) reflects the composition of the air mass revealed by the temperature analysis.

The echoes caused by turbulent mixing and the strong thermal gradient in the protruding nose are apparent below 200 m from 1638 to 1641. From 1642 to 1645 strong echoes appear along the boundary between the warm and cold air and weak echoes appear within the uniform cold air mass. Strong turbulent mixing behind the head from 1645 to 1647 is suggested by the strong echoes along the backside of the head from the surface upward to the 100 m level. The temporary increase in the depth of the cold air mass at 1649 can also be seen as an echo-free area surrounded by stronger echoes. Indicative of the fine resolution of the acoustic radar observations is the clear area visible below 220 m at 1645. This clear area resulted from a temporary increase in the depth of the cold air. This feature is barely discernable in the temperature analysis (Fig. 8b) due to insufficient resolution of the temperature sensors. The strong echoes between 50 and 150 m at 1644 occurred simultaneously with vertical velocities of -1.3 m sec^{-1} at the 177 m level. No evidence of the presence of cold air appears in either the analyses or the acoustic radar record after 1653. Acoustic radar echoes were limited to the lower levels, as they were prior to the first influx of cold air.

Case II

On 8 August 1972 a cold front, pushed southward by a Canadian airmass which was extremely cold for the season, was crossing Oklahoma. The cold front passed through the Oklahoma City area in the early afternoon and then stalled out in southern Oklahoma. During the early afternoon thunderstorms were occurring both along the front in southern Oklahoma and south of the front in western Texas. The 850-mb chart for 1800 CST (Fig. 9b) showed a weak trough extending from a low centered over Michigan to northeast Oklahoma to the Big Bend area of Texas. A high extended from north to south from western South Dakota to the Texas Panhandle. By 0000 CST 9 August (Fig. 9a) a minor wave had formed on the front with a weak surface low centered in southwest Oklahoma. By this time the area of thunderstorm activity had spread north of the front across Oklahoma.

One of these thunderstorms reached the acoustic radar site at 2318 CST. The cold outflow from this thunderstorm provides an interesting contrast to that reported in Case I. This thunderstorm was much less severe than that in Case I and no hail or high winds were reported. There was no sharp pressure jump associated with this thunderstorm, although a surface pressure rise of 1.2 mb did occur from 2230 to 2305 CST. After the initial rise, the surface pressure remained steady until

the onset of the cold air outflow at 2318, at which time a further rise of 0.1 mb occurred, followed by a drop of 0.2 mb.

There was no strong, sudden wind shift (Fig. 10d) preceding the cold air outflow, although a minor shift did occur at 2316 CST. Wind speed data (Fig. 10c) shows that a definite wind speed maximum did occur coincident with the influx of cold air at 2320 CST, but was weaker and less organized than in the 27 June case. The wind speed maximum in this case also was significantly retarded near the ground, although a minor maximum occurred at 2319 CST followed by a relative minimum before the major maximum occurred at 2319 CST. The speed maximum occurred at 177 m at 2320 CST. A definite wind speed minimum preceded the maximum in the lower levels. The high variability of wind speeds in the lower levels from 2318 to 2323 CST is indicative of strong turbulent mixing along the leading edge of the cold air near the surface.

The influx of cold air shows up most clearly in the acoustic radar facsimile record (Fig. 10b). Both the temperature analysis and acoustic radar echoes show the boundary of the cold air to be almost vertical. Acoustic radar echoes show the maximum height of the cold air to be 600 m. The initial temperature drop as revealed by the temperature analysis (Fig. 10b) was 3.5C near the surface, but decreased to 0.5C at the top of the

tower. The cold air was significantly retarded near the surface.

Strong positive vertical motions were observed immediately preceding the cold air influx with a maximum vertical velocity of 1.7 m sec^{-1} at 444 m. Downward vertical motions characterized the region immediately following the influx with a maximum of -1.3 m sec^{-1} at 444 m. As in Case I the strong downward motions are coincident with a thermal maximum. This thermal maximum may be observed in the temperature analysis in a period centered around 2326 CST. The maximum height of acoustic radar echoes gradually lowered during this period from 600 m at 2320 CST to 250 m at 2332 CST. The strong acoustic echoes within the body of the cold air indicate strong turbulent mixing. This indication is confirmed by strong vertical motions within the cold air mass.

The area of strong echoes surrounding relatively weak echoes on the acoustic radar facsimile record which reaches a height of approximately 530 m at 2340 CST shows up only weakly in the temperature data. The darker returns correspond to areas of cooler air where mixing is occurring with the warmer ambient air. The relatively weak returns in the center are revealed by the temperature data to correspond to a relatively homogeneous area of warmer air. From 2340 CST until the rain

began shortly after 0000 CST returns were weak and confined below 400 m. There were no further significant influxes of cold air during this period. The dark black bands on the acoustic radar record after 0000 CST and the completely dark area occurring after 0015 CST are caused by noise from rain striking the antenna.

CHAPTER IV

NOCTURNAL INVERSIONS

Case I

Following the thunderstorms of 8-9 August 1972 reported in Chapter III, another interesting situation occurred. The surface low which had formed on the front (Fig. 9a), after expanding northwestward and weakening somewhat (Fig. 9c), began moving eastward along the front. The air above the surface position of this low was much warmer than the air to the east or west, but the difference was barely noticeable at the surface because of modification of the air near the surface by cold outflow from thunderstorms in the area. By 0500 CST the Oklahoma City area had come under the influence of this low. Surface pressure at the WKY tower dropped 1.8 mb during the period 0445 to 0510 CST. Cold air from the west penetrated the southern portion of the low at this time and the low began moving northeastward. By 0600 CST the center of the low had passed to the west of Oklahoma City and by 0700 CST the low had completely dissipated with cooler air dominating the entire area.

After the rainfall ended at 0340, a weak inversion extended from the surface to approximately 300 m (Fig. 11b). Strong turbulent mixing within the inversion caused strong echoes to appear below the 300 m level in the acoustic radar record for this period (Fig. 11a).

The first indication of the advection of warm air can be seen on the acoustic radar record at 700 m at 0350 CST. The boundary between warmer and cooler air was marked by a thin line of dark echoes. These echoes reveal turbulent mixing of the warm and cold air at the boundary. The movement of this boundary downward with time can be followed quite easily. The warmer air reached the 444 m level of the tower at 0410 CST (Fig. 11b). The height of the boundary between warm and cold air at 0410 was indicated by the acoustic radar record to be approximately 440 m. From this time onward the height of the boundary on the acoustic radar record and on the temperature record agree quite well. By 0510 CST the warm air had penetrated to the surface.

The maximum temperature rise was 5C at approximately 180 m. The temperature at the top of the tower rose approximately 3C while the surface temperature rose only 0.5C.

By inspecting Fig. 12a and Fig. 12b one can see the great amount of structure revealed in the acoustic radar record and

the high correlation between the acoustic radar record and temperature field. In Fig. 12a the dark trace below 100 m from 0515 to 0600 CST is indicative of turbulent mixing near the surface, while the bands of echoes above correspond to regions of strong temperature gradient within the inversion. The resolution of the temperature data is not great enough to reveal such detailed structure. However, it can be seen that the areas of strong temperature gradient that do appear in the temperature analysis correspond to areas of strong echoes on the acoustic record. For example, the perturbations occurring in the temperature field at approximately 0528 CST and at 0554 CST correspond to an increase in the maximum height of strong acoustic radar echoes.

At 0600 CST the return of the cold air began in quite a dramatic fashion. The cold air returned in a series of surges, each deeper than the surge that preceded it.

The first surge began at 0603 CST and reached a maximum height of approximately 470 m at 0609 CST. This surge appears in the acoustic radar record (Fig. 12a), as a peak of echoes, with strong echoes along its boundary and weaker echoes in its center. The layered appearance of the echoes at this time should be noted. Whether this layered structure is reflected in the temperature field cannot be determined because spacing of the sensors is inadequate for such fine resolution. The

temperature analysis (Fig. 12b) shows a maximum temperature drop of 4C at 150 m. The temperature near the surface dropped only slightly. Wind speeds (Fig. 12c) increased below 250 m and decreased above that level. Wind direction (Fig. 12d) showed a distinct shift from north-northeast to southeast below 250 m following the initial surge of cold air. The warm air returned from 0609 to 0615 CST, cooled slightly by mixing with the colder air. The maximum height of echoes dropped to 180 m at 0615 on the acoustic radar record. Temperatures at the 150 m level rose 3.3C. Again surface temperatures changed very little. Wind speeds increased above 150 m and decreased below that level. Wind directions changed back to the north-northeast at upper levels and to the northeast at lower levels.

The second surge of cold air began at 0615 CST; the mass of the cold air reached a maximum depth of 480 m at 0620 CST. Acoustic radar echoes were very strong along the interface between the warm and cold air during this time. The maximum temperature again changed very little. Wind speeds increased below 250 m and decreased above that level. Wind directions switched to the southeast below 300 m and remained northeasterly above that level.

Warmer air reappeared above 200 m during the period 0620 to 0626 CST. The air was 2 to 3C cooler than previously; this

suggests considerable mixing. Wind direction changes were confined to levels above 100 m.

The next surge of cold air brought cold air dominance to all levels of the tower. Temperatures began to increase slightly in the lower levels due to surface heating. The wind direction remained fairly constant from the southeast following this surge. Wind speeds remained variable in the upper levels and the gustiness decreased slightly in the lower levels. Strong acoustic radar echoes at all levels after this time indicates turbulent mixing in the cooler air.

Case II

At 0001 CST on 26 June (Fig. 13a), a weak quasi-stationary front was oriented in an east-west direction along the Kansas-Oklahoma border. A surface low was centered in western Oklahoma with a trough extending south-southwestward to the Big Bend area of Texas. An 850-mb trough (Fig. 13b) was oriented north-south on a line extending from western North Dakota into the Texas Panhandle. Extensive thunderstorm activity was occurring in Kansas and eastern Oklahoma. Winds in the Oklahoma City area were from the southeast. Temperatures measured at the WKY tower (Fig. 14c) showed a slight decrease from the surface to the 444 m level. With the approach of the surface low and

the formation of a cut-off low at 850 mb over the Texas Panhandle, winds switched to the southwest at all levels and increased in speed (Fig. 14d). This caused advection of warmer, drier air aloft. The acoustic radar record just prior to midnight showed weak echoes which extended from the surface to 700 m. These echoes indicated turbulent mixing at all levels. Soon after midnight, the intensity of returns increased (Fig. 14a). This increase was reflected in the analyses of tower data as rapid fluctuations with time of temperatures (Fig. 14d) and vertical velocity. The upper limit of strong echoes coincided with the base of an inversion which had formed aloft. This inversion began propagating slowly downward as warm air advection increased the temperature at lower levels. The base of the inversion passed the 444 m level of the tower at approximately 0030. From that time until 0700 CST temperature increased with height at all levels of the tower. Strong echoes continued to be received in the region below the base of the inversion, but only weak echoes were received from the area above the base. The base of a second inversion appeared at the 600 m level of the acoustic radar trace at 0130 CST. This inversion also propagated downward until it joined the base of the second inversion at 300 m at 0300 CST (Fig. 14b). It appeared as a thin line of echoes on the facsimile record;

only weak echoes were received from the area between it and the base of the lower inversion. Examination of the tower data revealed that this second inversion was much stronger than the first. It was accompanied by a low-level wind maximum (Fig. 14d) at its base of 16-18 m sec^{-1}. At 0300 a band of very strong echoes appeared on the facsimile record below the wind maximum. Weaker echoes were received in the area below this band of strong echoes. These strong returns were probably caused by turbulent downward mixing of the warm air. The turbulent mixing was probably, in turn, caused by the strong wind shear which overcame the stability of the layer. Above the wind speed maximum, returns were weak or nonexistent until 0630 CST (Figs. 15a and 15b).

Richardson numbers calculated for the layer below the wind maximum were consistently below 0.25, the criteria generally accepted for the onset of turbulence being $R_i = 0.25$. The wind speed maximum gradually lowered to 250 m (Fig. 15b) and remained there until approximately 0635 CST (Fig. 16b). It then began a slow rise and reached a height of approximately 300 m at 0715, immediately before the inversion broke down. Changes in height of the wind speed maximum are reflected in the acoustic radar record (Figs. 15b and 16a) as changes in height of the top of the area of echoes. At 0545 CST (Fig. 15b)

the first weak echoes from the base of a third inversion appeared at approximately 550 m. This third inversion also propagated downward and reached the 350 m level at 0630. The trace from this inversion appears as a layer of echoes approximately 50-100 m thick. Richardson numbers within the third inversion were strongly positive, so the echoes were probably not the result of scattering of the acoustic wave by turbulent fluctuations in the temperature field. The echoes were probably the result of specular reflection of the acoustic wave from the strong thermal gradient at the base of this inversion (approximately +7C per 100 m). Stronger echoes which were received from the base of this inversion from approximately 0650 to 0655 CST (Fig. 11a) possibly were caused by a temporary upward excursion of the wind speed maximum. Although there is slight evidence that this occurred, resolution of the wind speed analysis is insufficient to make the statement with any degree of certainty. The two areas of echoes almost merged during this period. A series of wave-like perturbations appeared in the echoes from the base of the upper inversion at 0700 CST. These perturbations are also visible in echoes from the lower layers and are reflected in the temperature analysis (Fig. 16b) as deformations of the temperature field. The cause of these perturbations is unknown. They were possibly the result of weak pressure jumps. Temporary cooling below the

base of the inversion during the first showing perturbation is indicated by the temperature analysis to be -0.5 to -0.8 C. Such cooling is entirely consistent with the adiabatic rise of an air parcel of 50 to 100 m or approximately the vertical extent of the perturbations. Also note that temperatures rise back to their former levels after the perturbations pass. The area of very weak returns below 150 m (Fig. 16a) probably reflects the slight rise in height of the maximum wind speed level (Fig. 16c), smaller wind shears in the layer, and the development of a weakly negative temperature gradient (Fig. 16b) below 150 m.

The entire inversion structure broke down chaotically at 0718. As can be seen from the temperature time section, temperatures at the top of the tower fell by 10C in 5 min. The surface pressure rose sharply from 0716 to 0720 CST with a total rise of 2 mb. The surface pressure remained fairly steady until 0735 CST, then dropped 0.5 mb from 0730 to 0735 CST. It rose back to the 0735 level at 0742 and remained fairly steady afterward. Temperatures, winds and vertical velocities were highly variable from 0718 to 0742 CST. Vertical velocities were highly variable from 0718 to 0742 CST. Vertical velocities were high (plus or minus 4.5 m sec^{-1} maximum) and isotherms were oriented essentially vertically from 0718 to 0735 and again from 0745 to 0748 CST. The facsimile record

for these periods shows bands of alternately strong and light echoes (Fig. 16a) extending throughout the entire height range of the radar. The curious spiral effect noted in the acoustic radar echoes from 0730 to 0735 CST occurred during a period of strongly positive vertical velocities and a distinct reappearance of warmer air at all levels of the tower (Fig. 16b). Horizontal wind speeds (Fig. 16c) during this period were highly variable, with a definite maximum at higher levels and a distinct minimum at lower levels. The period of strong returns from 0745 to 0748 CST was also coincident with strong upward motion and warmer temperatures at all levels. The period of relatively weak echoes from 0735 to 0745 was characterized by downward motion, cooler temperatures at all levels, and a more horizontal orientation of the isotherms, indicative of less turbulent mixing during this time.

After 0751 CST the time section of temperature (Fig. 16b) shows a steady decrease in temperature with height. The lapse rate was, in fact, dry adiabatic. Acoustic radar echoes (Fig. 16a) were weak after 0751 CST, the only strong echoes being from small thermals which began to form in the lower 100 m.

Complete destruction of such a stable boundary layer structure (temperature gradient at the 355 m level was 6 to 7 C per 100 m 30 min before breakdown began) presents the question

of what mechanism caused the destruction. Several theories were considered and discarded in turn.

The first mechanism considered was a frontal passage, since there was a front to the north of the station at the time. Facts argued against a frontal passage at this time, however. Winds remained from the northwest for a period of only about 30 min and were highly variable during the whole period, then switched back to the southwest after 30 min. Furthermore there is evidence of a frontal passage at 0930 CST, resulting in a prolonged period of north winds, a reduction in surface temperature rise, and a surface pressure rise. A pressure jump was the next mechanism considered (Tepper, 1955), since there were intense thunderstorms occurring in northeast Oklahoma and Kansas during this time, although the level of activity was diminishing. A pressure jump was ruled out, since an elevation of the height of the inversion with the resultant adiabatic cooling of the air below could in no way have produced the adiabatic lapse rate present after 0751.

There was no evidence of passage of a convergence zone or instability line. Nor was there evidence of the passage of an upper air trough. The surface low center remained to the west of Oklahoma City during the entire period. The most plausible explanation lies in the cold air produced by

thunderstorms to the north. At 0700 CST there were two meso-highs in southern Kansas with central pressures of 1013 and 1014 mb. An isotherm analysis showed that there was a definite extension of cold air into northwestern Oklahoma. Central pressure in both meso-highs dropped by 2-3 mb from 0700 to 0800 CST, accompanied by surface pressure rises at stations in northern and central Oklahoma. Evidence indicates that some of the cold air pushed out ahead of the front, destroying the inversion. The main body of cold air remained behind the front and provided the mechanism for reintensification of the front, which had been stationary for some time, enough so that it pushed into southern Oklahoma. Due to strong surface heating, the colder air was hardly noticed at the surface, resulting only in a decrease in the rate of temperature rise.

CHAPTER V

SUMMARY AND CONCLUSIONS

The results of the studies reported in previous chapters indicate that, as predicted by theory, the major sources of acoustic radar echoes in the backscatter mode are strong thermal gradients and turbulent fluctuations of temperature. The pattern and intensity of returns can be related directly to the temperature field in the case of returns from strong thermal gradients and to the temperature, wind, and stability fields in the case of returns from turbulent fluctuations of temperature. The amount of fine structure revealed by acoustic radar records cannot be attained by conventional instruments.

The attempt made here to relate the boundary layer processes revealed by the acoustic radar and tower data to causitive synoptic processes was only partially successful due to lack of resolution of the synoptic data available. However, it has been shown that such associations can provide valuable insight into boundary layer processes. Further studies using mesonetwork data would be desirable.

The acoustic radar shows great promise in thunderstorm outflow studies. As shown in Chapter III the structure of gust fronts can be quite different depending on the intensity and areal coverage of the storms, storm path, and other factors. The thunderstorm outflow of 27 June 1972 showed significant correlation with Charba's (1972) gust front model. The case study of 8-9 August 1972 showed less correlation, probably due to the lack of the severity of the storm and interaction with outflow from other storms in the immediate area. This result is to be expected since Charba's model predicates a strong, organized thunderstorm system rather than a broad area of weak or moderate thunderstorm activity as was the case on 8-9 August 1972.

The study and monitoring of inversions using the acoustic radar has direct application to air pollution meteorology. Acoustic data reveal areas of strong thermal gradients, mixing areas, and the exact time of inversion breakdown. Further studies should be carried out in order to discover the mechanisms involved in inversion breakdown.

Although this study has been limited to qualitative interpretation of acoustic radar data, capabilities of the acoustic radar are not limited to qualitative data only. Determination of the structure constants of wind and temperature

would enable the collection of quantitative data on both winds and temperatures, given the proper equipment configuration. Vertical velocities can be determined using the Doppler shift of the acoustic returns. Thus the acoustic radar holds the potential of becoming an invaluable asset in boundary layer studies and monitoring.

REFERENCES

Benjamin, T. B., 1968: Gravity currents and related phenomena. 2, J. Fluid Mech., 31, 209-248.

Beran, D. W., Little, C. G., and Willmarth, B. C., 1971: Acoustic Doppler Measurements of Vertical Velocities in the Atmosphere. Nature, 230, 160-162.

Berson, F. A., 1958: Some measurements of undercutting cold air. Quart, J. R. Meteor. Soc., 84, 1-16.

Carter, J. K., 1970: The meteorological instrumented WKY-TV tower facility. National Severe Storms Laboratory, Tech. Memo. No. 50, 18 pp.

Charba, J. P., 1972: Gravity-Current Model Applied to Analysis of Squall-Line Gust Front. Ph.D. dissertation, University of Oklahoma.

Cronenwett, W. T., G. B. Walker, and R. L. Inman, 1972: Acoustic Sounding of Meteorological Phenomena in the Planetary Boundary Layer, accepted for publication in J. of Applied Meteo.

Derr, V. E. and C. G. Little, 1970: A comparison of Remote Sensing of the Clear Atmosphere by Optical, Radio, and Acoustic Radar Techniques. Applied Optics, Vol. 9, No. 9.

Fujita, T., 1959: Precipitation and cold air production in mesoscale thunderstorm system. J. Meteor., 16, 454-466.

Gilman, G. W. Coxhead, H. B., and Willis, F. H.; 1946: Reflection of Sound Signals in the Troposphere. J. of the Acoustical Soc. Am., 18, 274-283.

Kallistratova, M. A., 1961: Experimental Investigation of Sound Wave Scattering in the Atmosphere. Trudy Inst. Fiz. Atmos., Atmos. Turbulentnost, No. 4, 203-256.

Little, C. G., 1969: Acoustic Methods for the Remote Probing of the Lower Atmosphere. Proc. I.E.E.E., 57, 571-578.

McAllister, L. G., 1968: Acoustic Sounding of the Lower Troposphere. J. Atmospheric Terrest. Phys., 30, 1439-1444.

McAllister, L. G., Pollard, J. R. Mahoney, A. R., and Shaw, P. J. R., 1969: Acoustic Sounding--A New Approach to the Study of Atmospheric Structure. Proc. I.E.E.E., 57, 579-587.

McAllister, L. G., and J. R. Pollard, 1969: Acoustic Sounding of the Lower Atmosphere. Proceedings of the Sixth International Symposium on Remote Sensing of Environment, Vol. 1, pp 436-450.

Monin, A. S., 1962: Characteristics of the Scattering of Sound in a Turbulent Atmosphere. Akusticheskiy Zhurnal, Vol. 7, 457-461 (Sov. Phys. Acoustics, Vol. 7, pp 370-373.)

Plate, E. J., 1971: Aerodynamic Characteristics of Atmospheric Boundary Layers. United States Atomic Energy Commission, Division of Technical Information, Oak Ridge, Tenn.

Tatarski, V. I., 1961: Wave Propagation in a Turbulent Medium. Translated by R. A. Silverman, Dover Publications.

Tepper, M., 1950: A proposed mechanism of squall lines: The pressure jump line. J. Meteor., 7, 21-29.

Tyndall, J., 1875: Sound. Appleton Co., London, 3 ed., Ch 7.

Wescott, J. W., Simmons, W. R., and Little, C. G., 1970: Acoustic Echo-Sounding Measurements of Temperature and Wind Fluctuations. Essa Technical Memo. ERLTM-WPL 5, 24 pp.

Table 1

Acoustic Radar Parameters

Range	700 meter
Frequency	1500 Hertz
Acoustic pulse power	30 watts
Pulse length	42.6 milliseconds
Receiver bandwidth	70 Hertz
Antenna diameter	1.21 meter

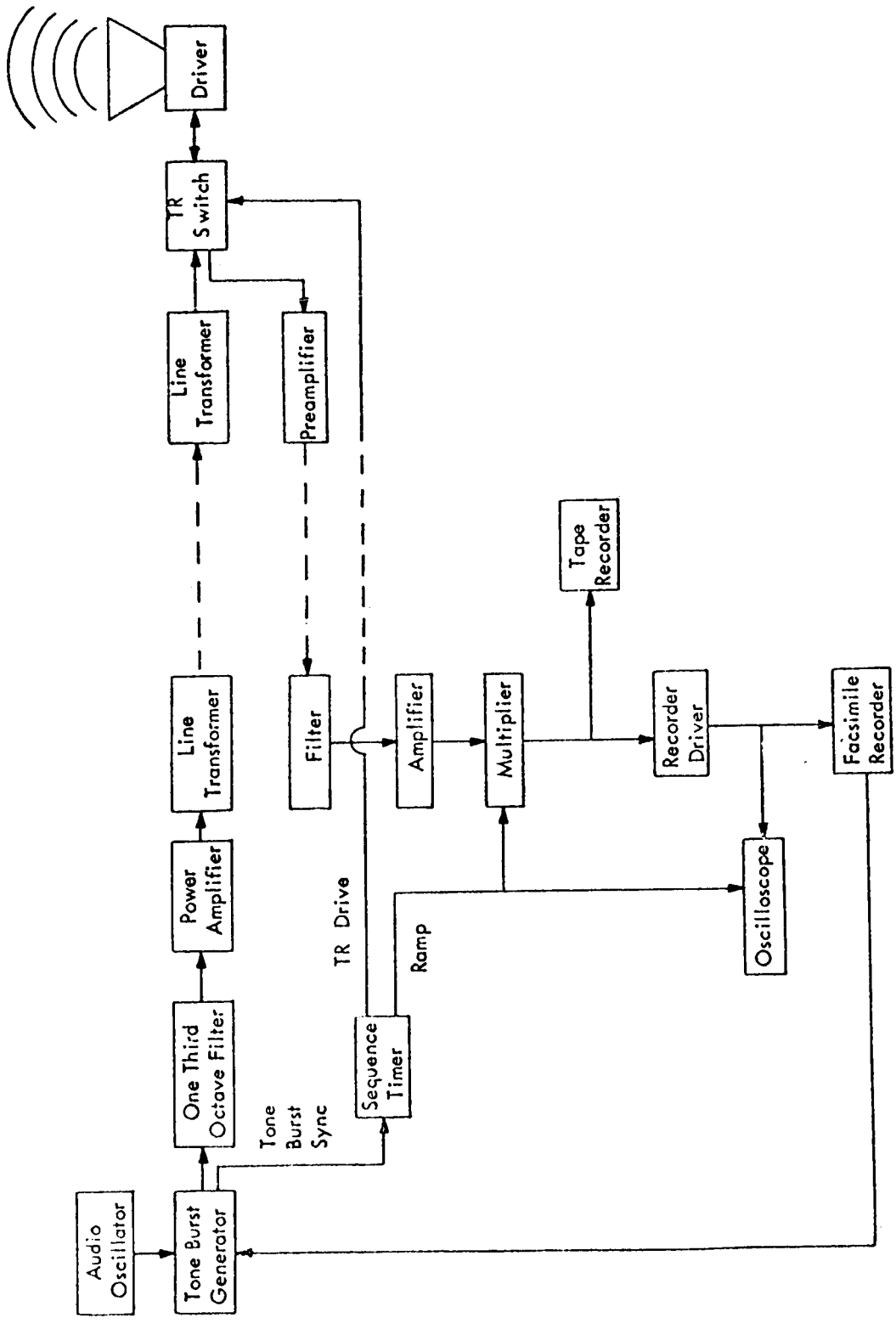

Fig. 1. Block Diagram of the Acoustic Radar (Cronenwett et al, 1972).

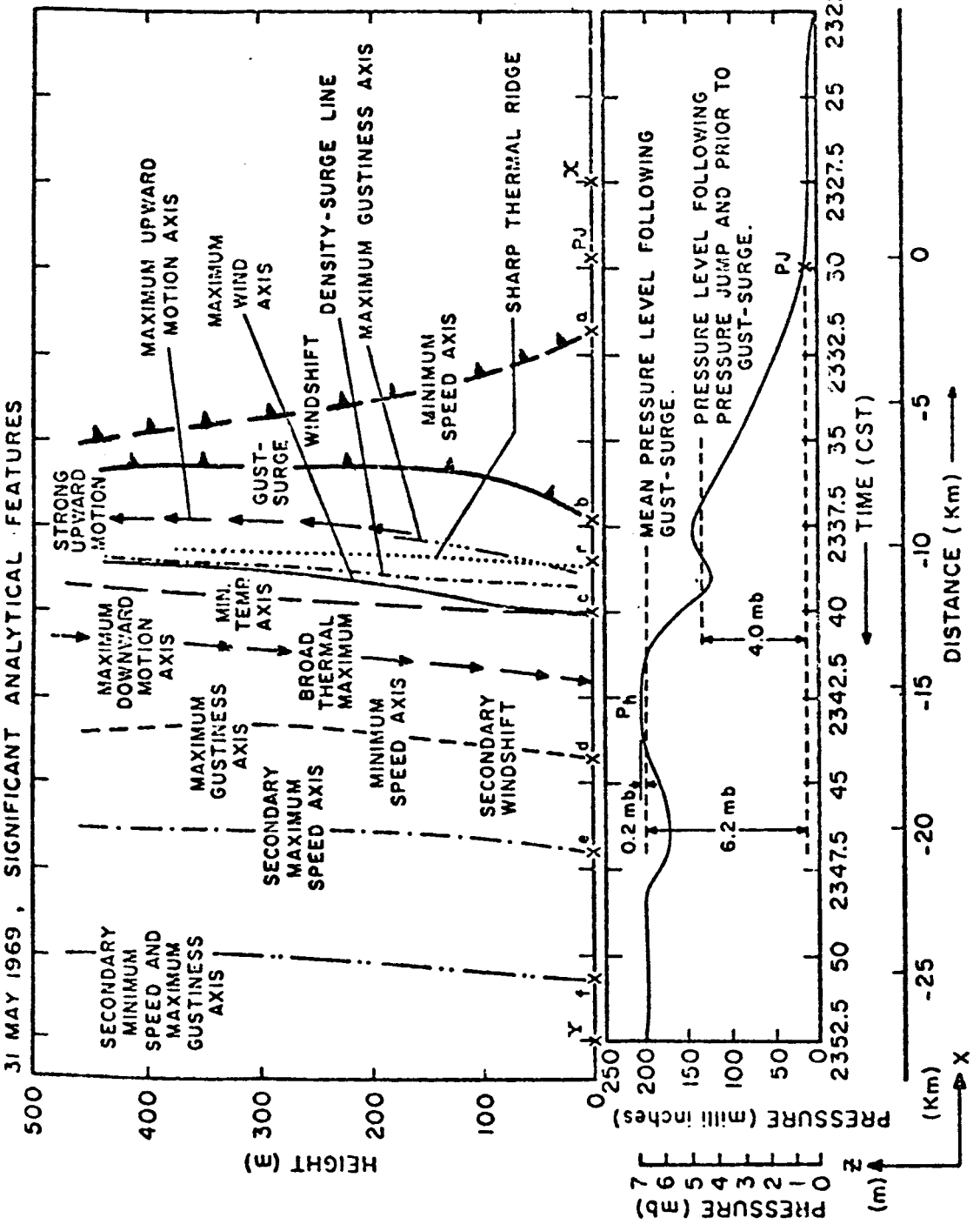

Fig. 2. Schematic of the important analytical features of the wind and thermal structure of the windshift and gust front (upper). The surface pressure profile is also shown (lower) (Charba, 1972).

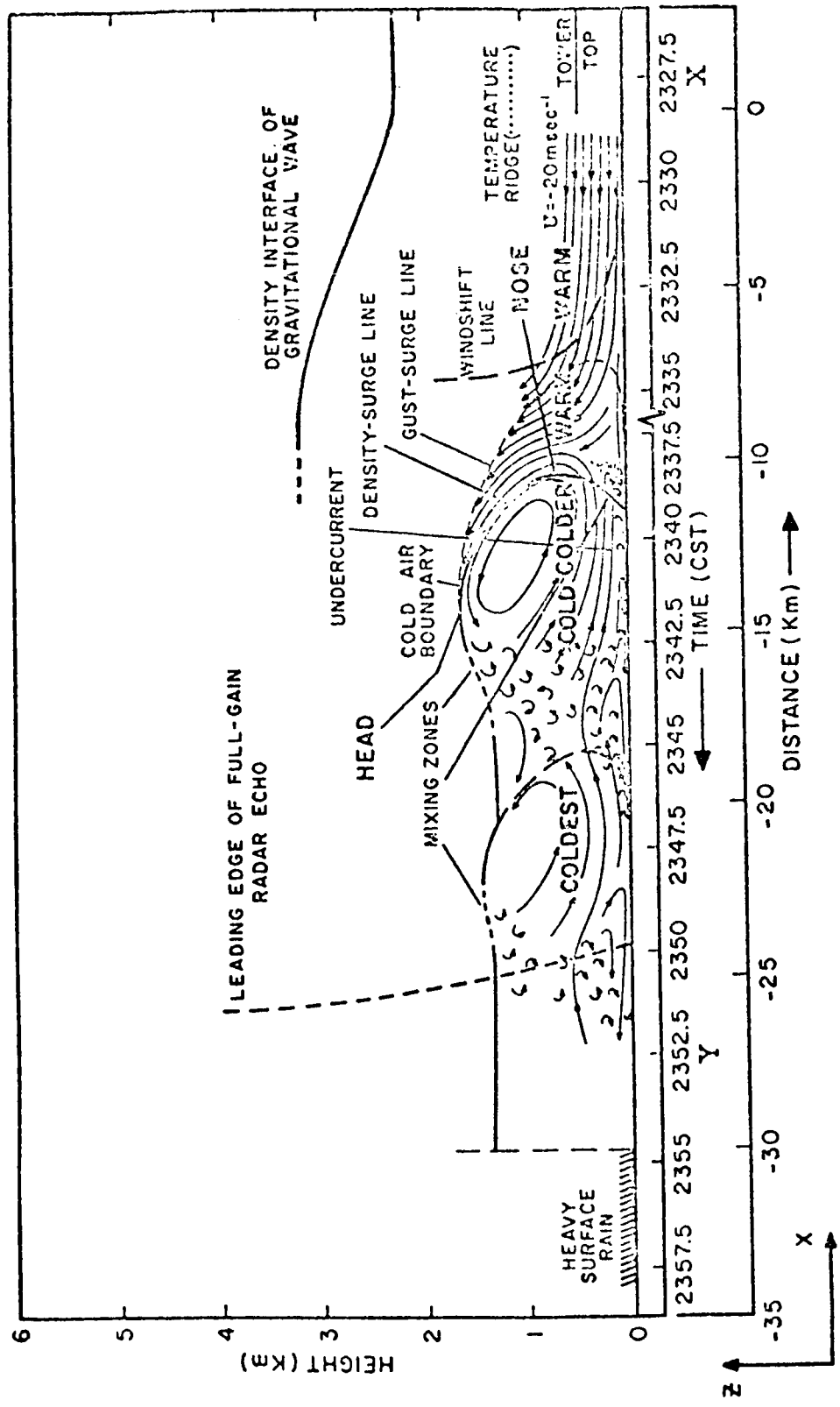

Fig. 3. A composite schematic model combining the features of the analyzed and deduced structure of the windshift and gust front leading the squall line of 31 May 1969 (Charba, 1972).

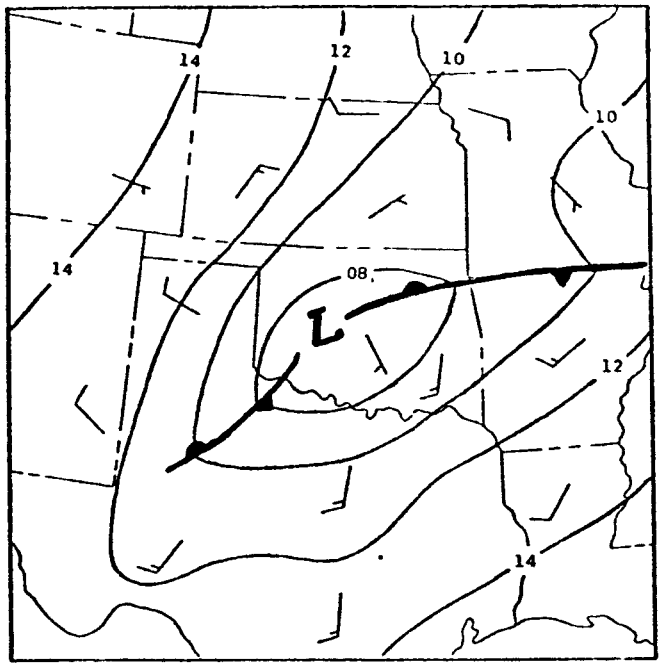

Fig. 4. Surface analysis for 1100 CST 27 June 1972 (pressure contours in millibars, i.e., 08 = 1008 mb).

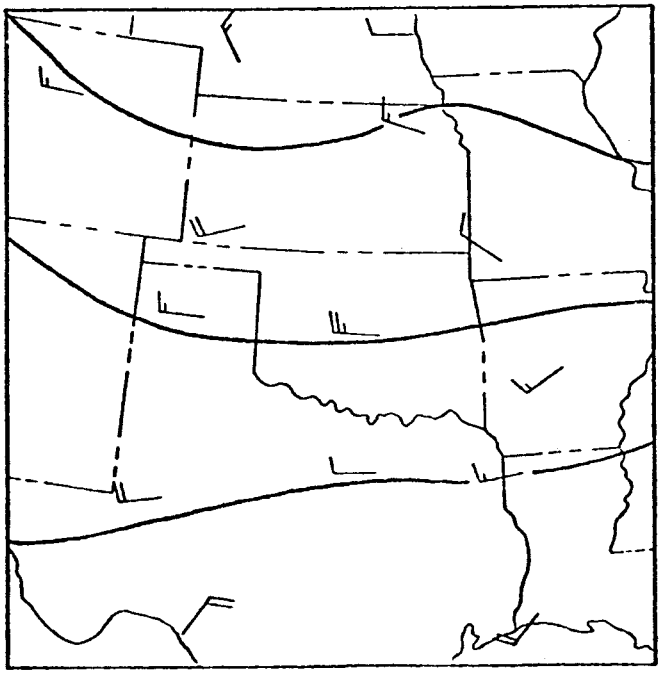

Fig. 5. Height contour patterns at the 700 mb level for 0600 CST 27 June 1972 (contour interval is 60 m).

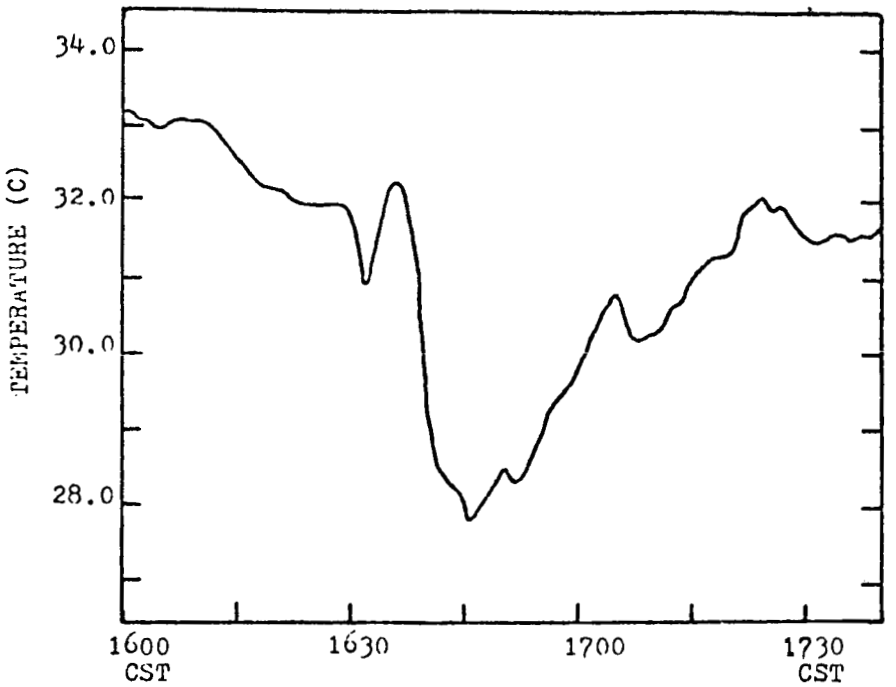

Fig. 6. Surface temperature (degrees C) at WKY tower for 27 June 1972.

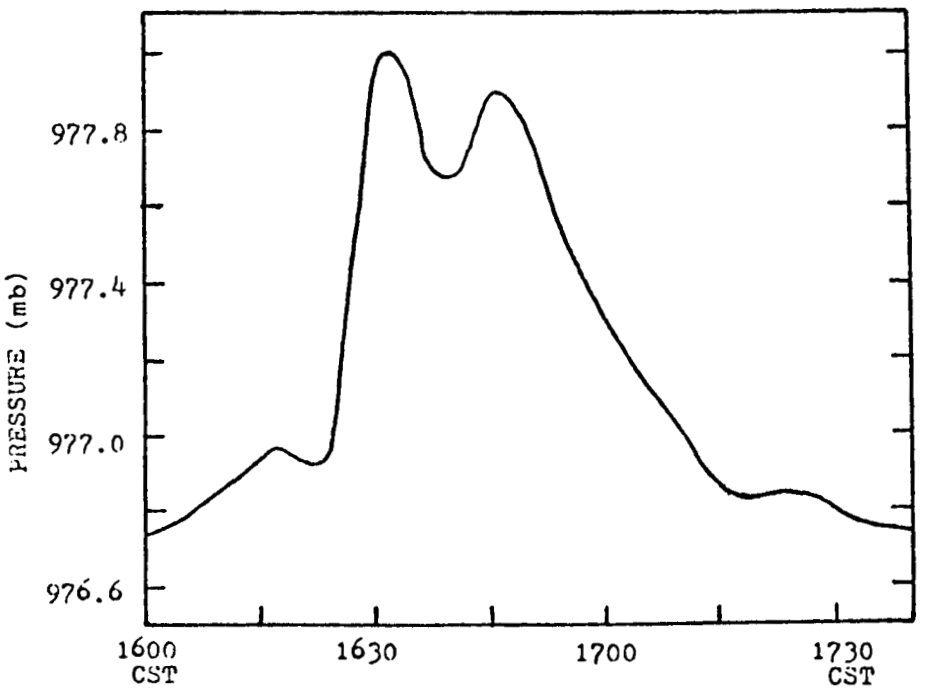

Fig. 7. Microbarograph trace (pressure in millibars) at WKY tower for 27 June 1972.

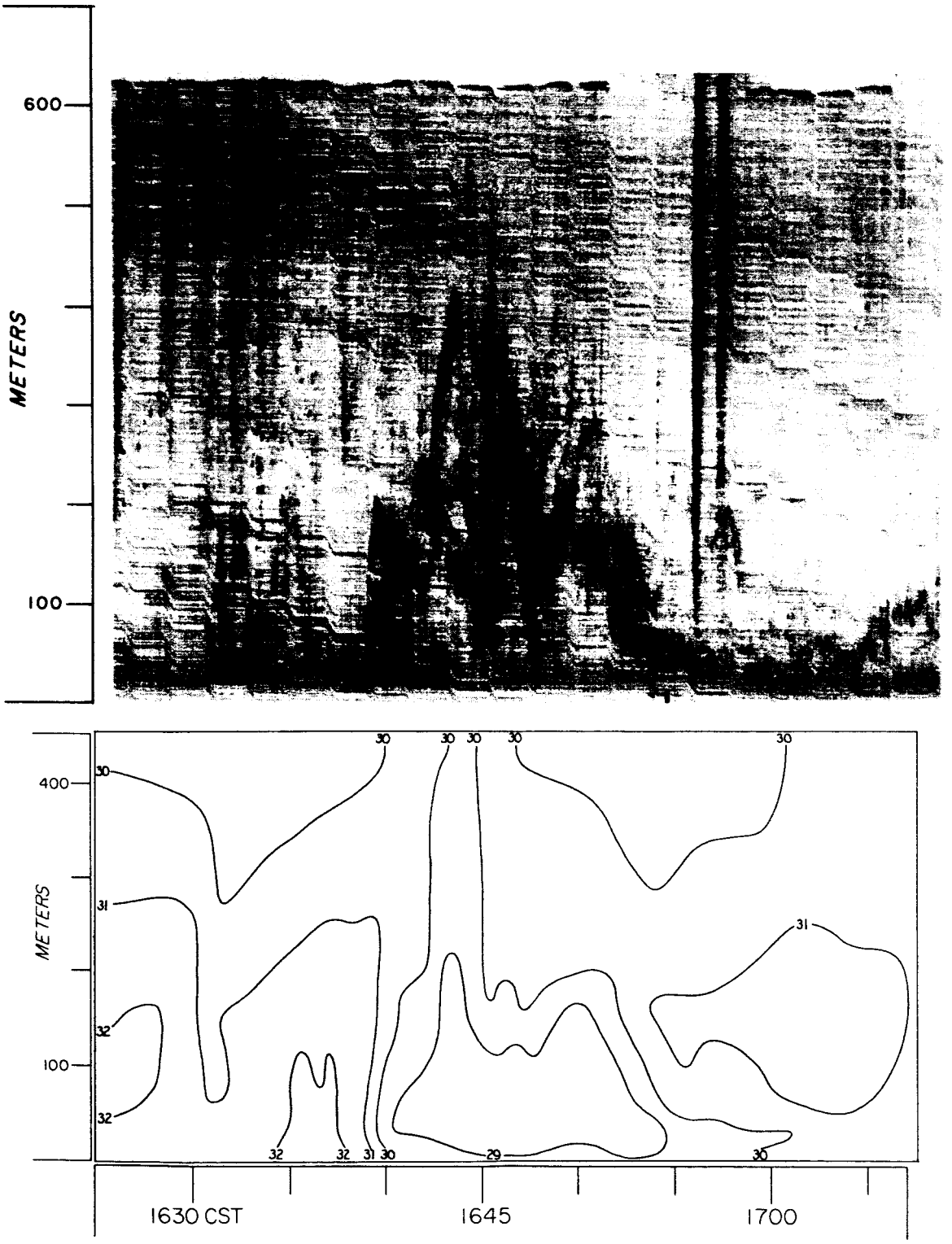

Fig. 8. Acoustic radar facsimile record (a) and time section of temperature (degrees C) (b) for 1625-1707 CST 27 June 1972.

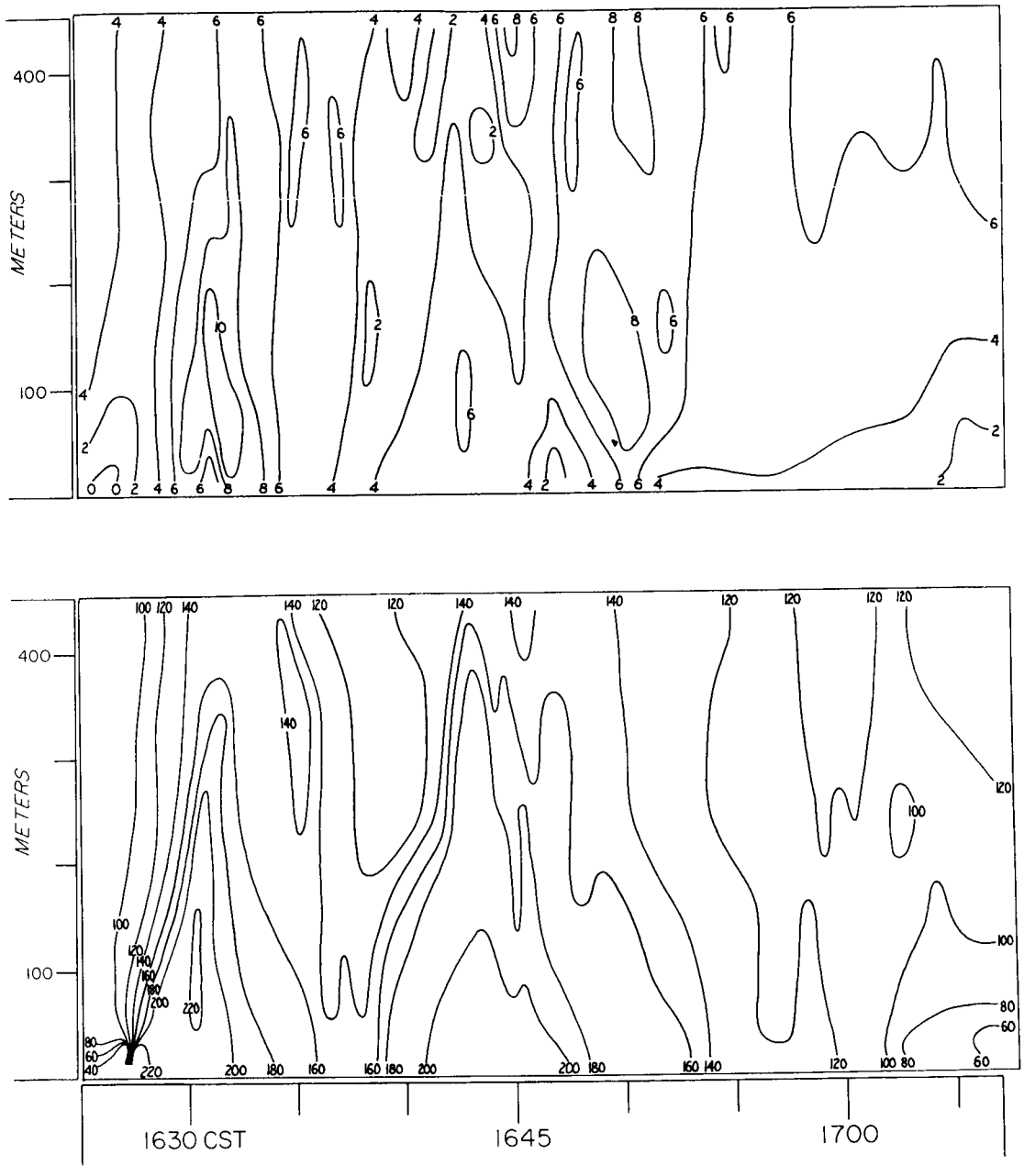

Fig. 8. Time section of wind speed ($msec^{-1}$) (c) and wind direction (degrees) (d) for 1625-1707 CST 27 June 1972.

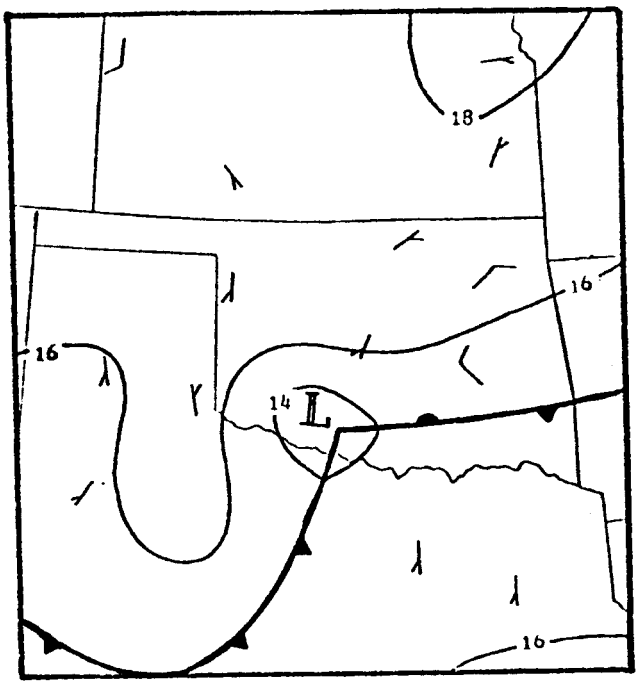

Fig. 9a. Surface analysis for 0000 CST 9 August 1972 (pressure contours in millibars, i.e., 08 = 1008 mb).

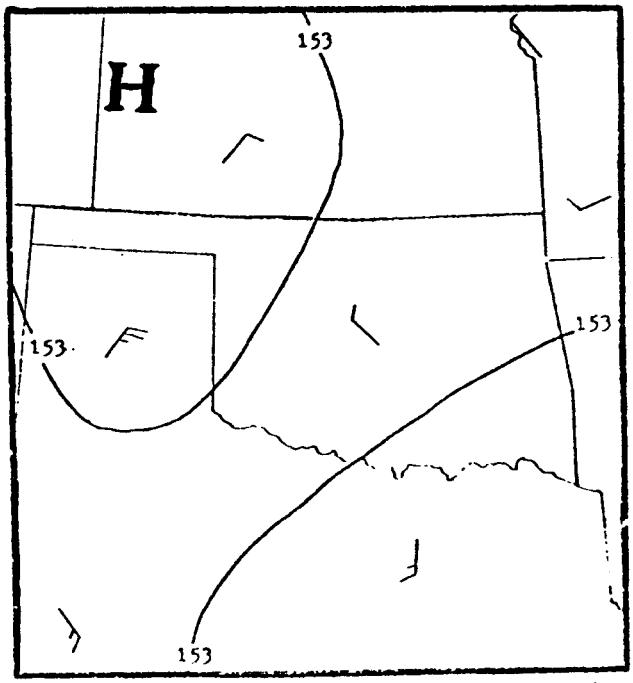

Fig. 9b. Height contour patterns at the 850 mb level for 1800 CST 8 August 1972 (contour interval is 30 m).

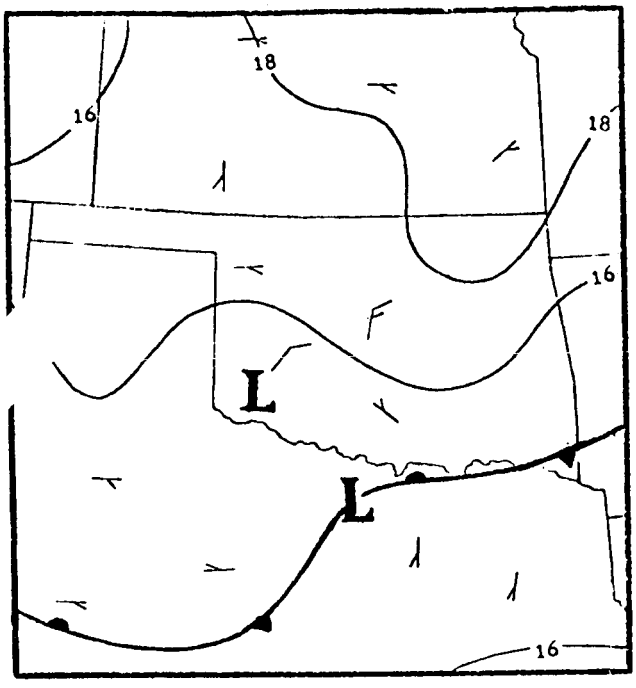

Fig. 9c. Surface analysis for 0300 CST 9 August 1972 (pressure contours in millibars, i.e., 08 = 1008 mb).

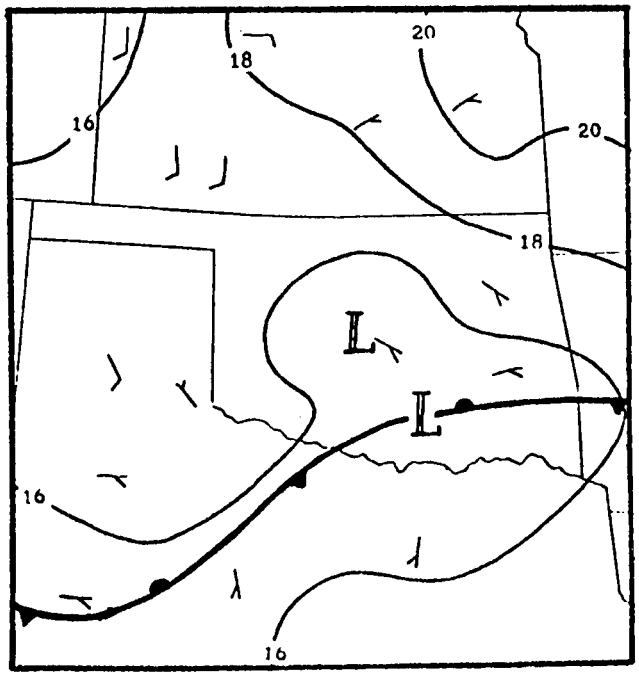

Fig. 9d. Surface analysis for 0600 CST 9 August 1972 (pressure contours in millibars, i.e., 08 = 1008 mb).

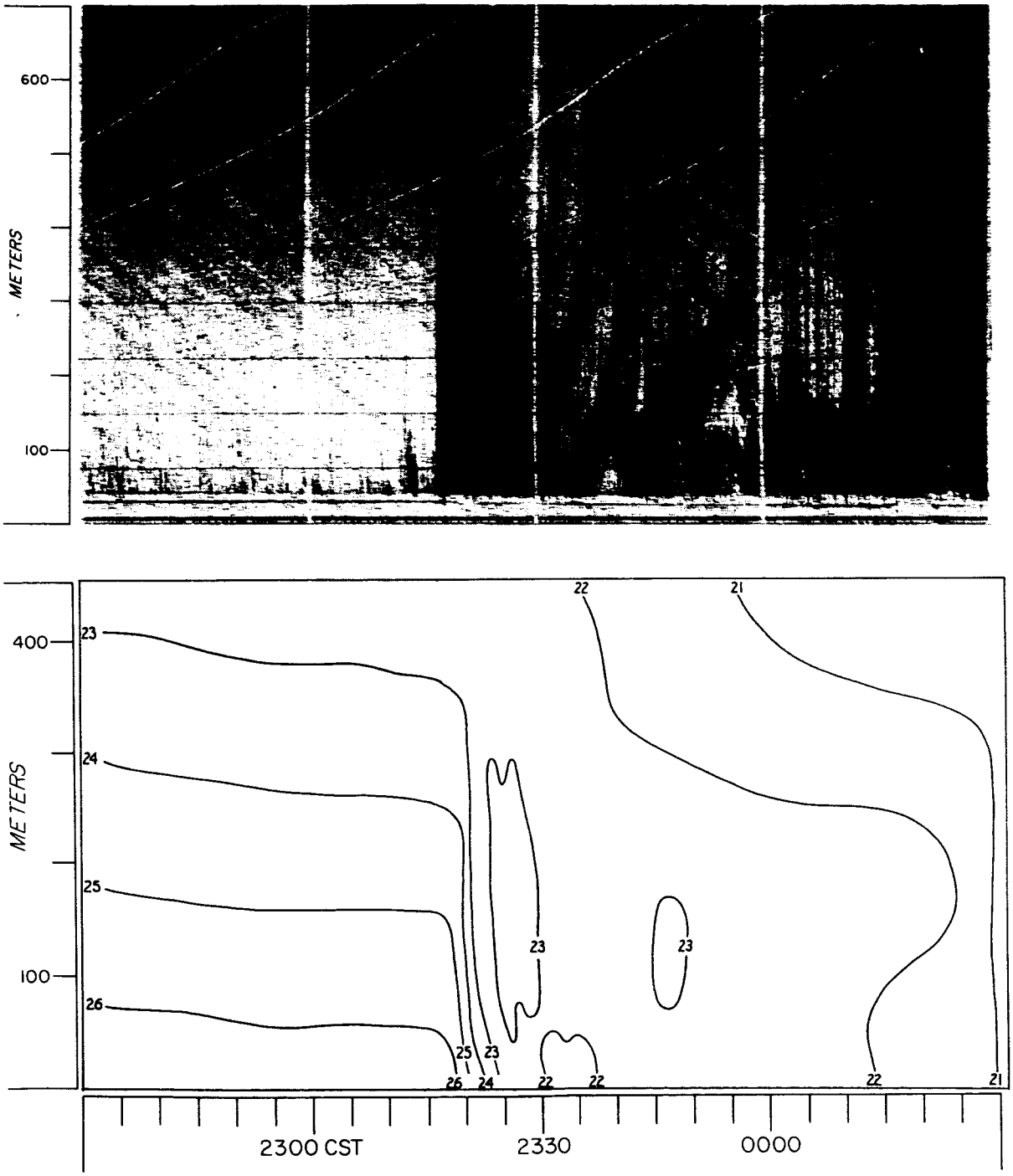

Fig. 10. Acoustic radar facsimile record (a) and time section of temperature (degrees C) (b) for 2230-0030 CST 8-9 August 1972.

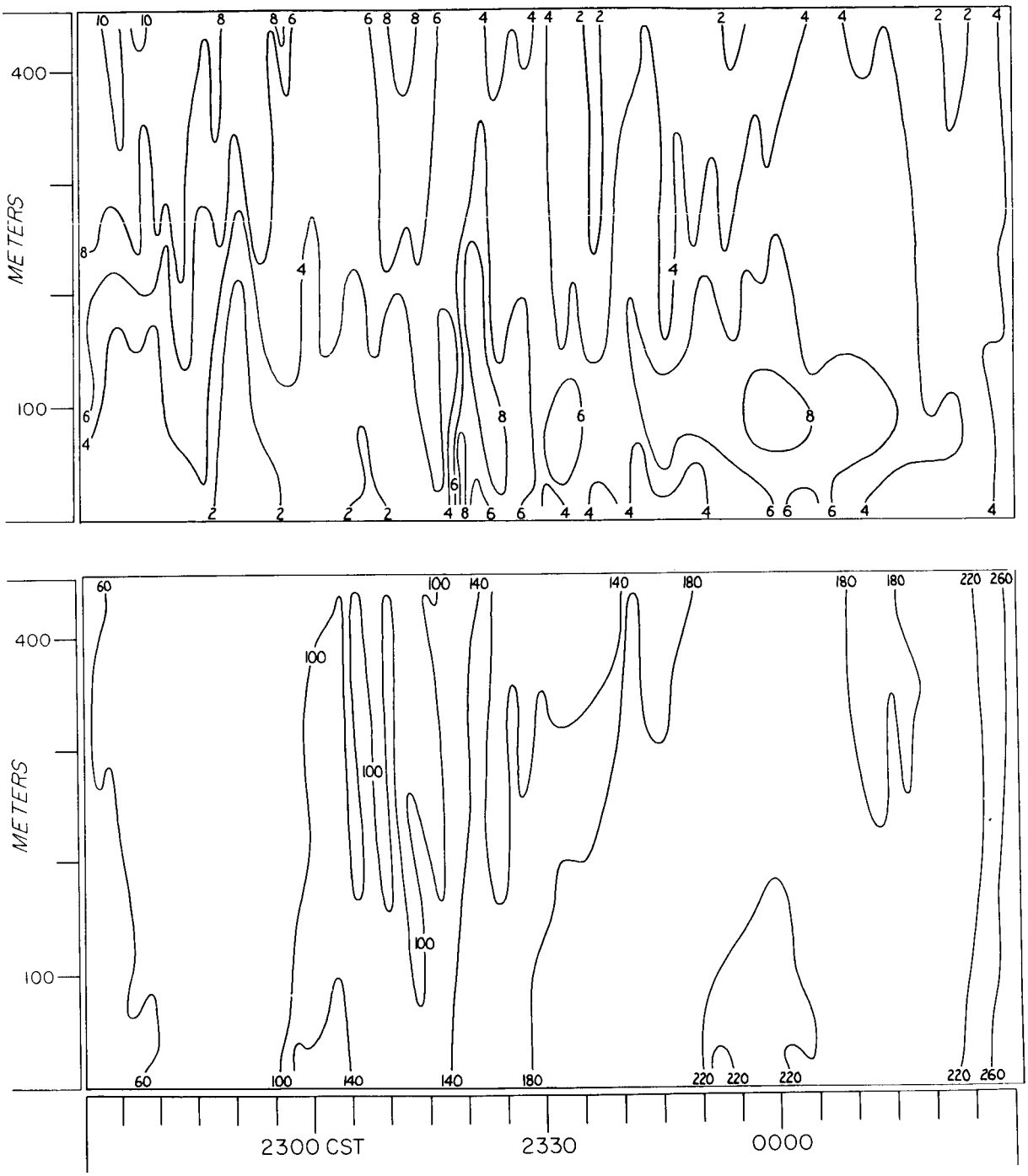

Fig. 10. Time section of wind speed ($msec^{-1}$) (c) and wind direction (degrees) (d) for 2230-0030 CST 8-9 August 1972.

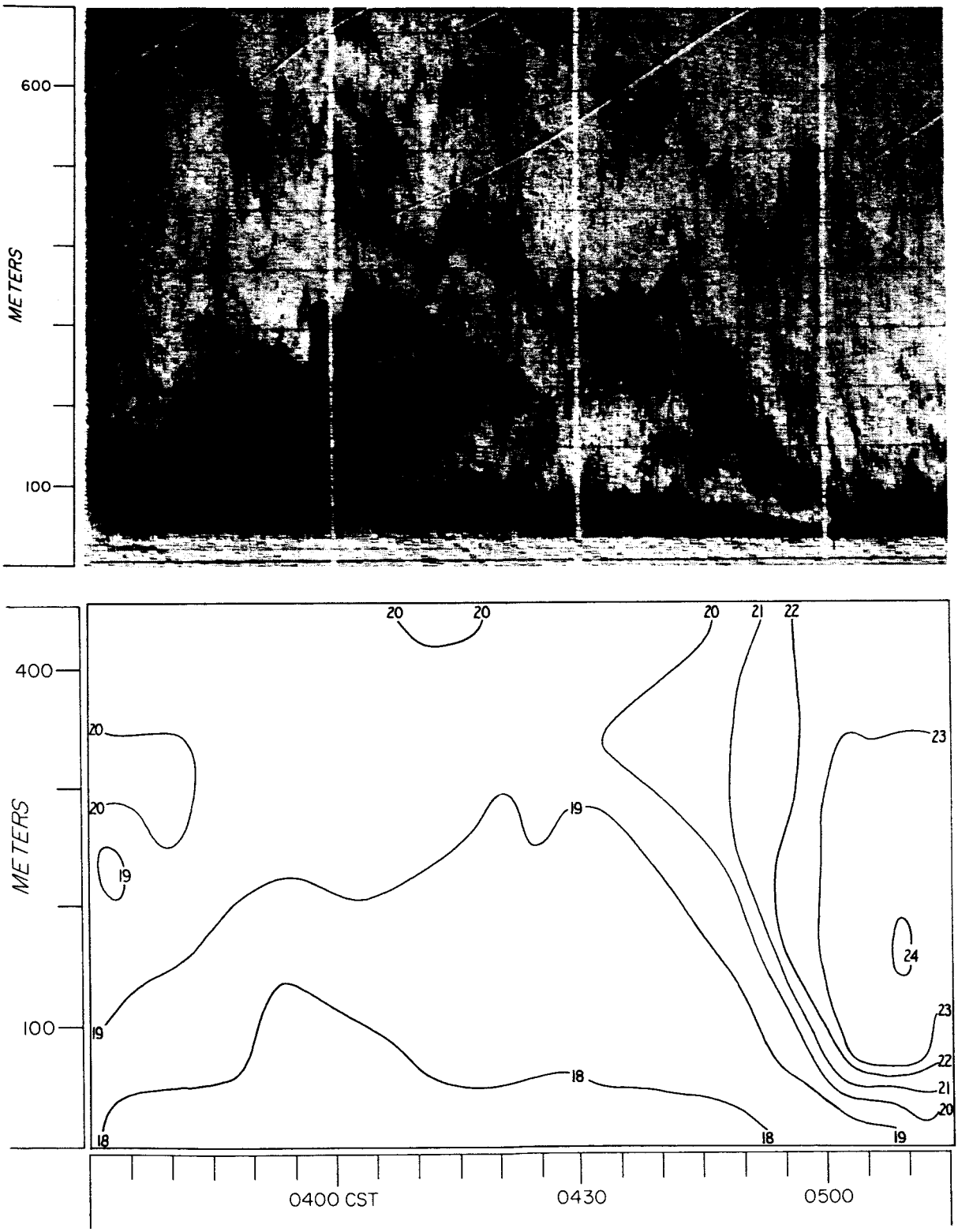

Fig. 11. Acoustic radar facsimile record (a) and time section of temperature (degrees C) (b) for 0330-0515 CST 9 August 1972.

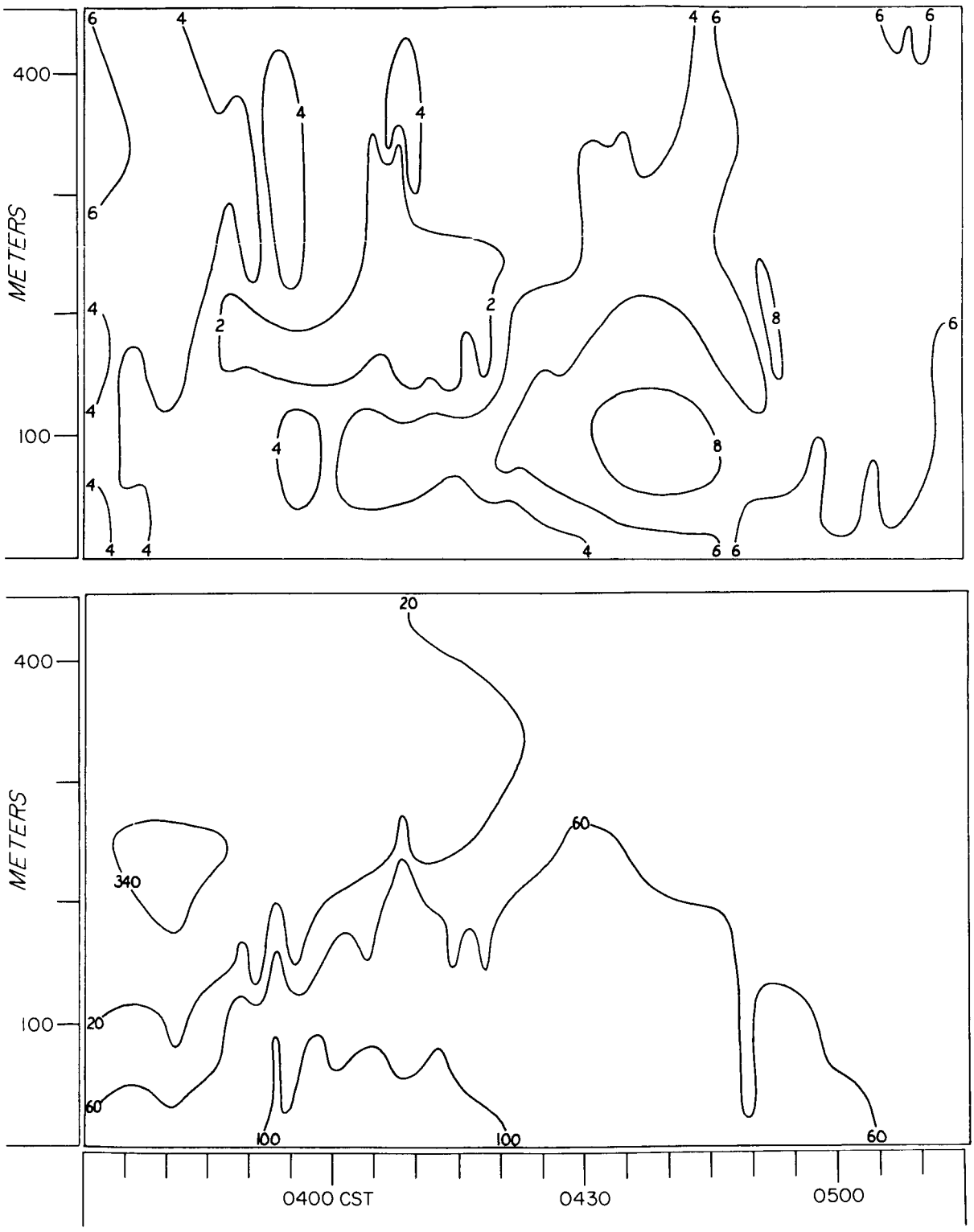

Fig. 11. Time section of wind speed ($msec^{-1}$) (c) and wind direction (degrees) (d) for 0330-0515 CST 9 August 1972.

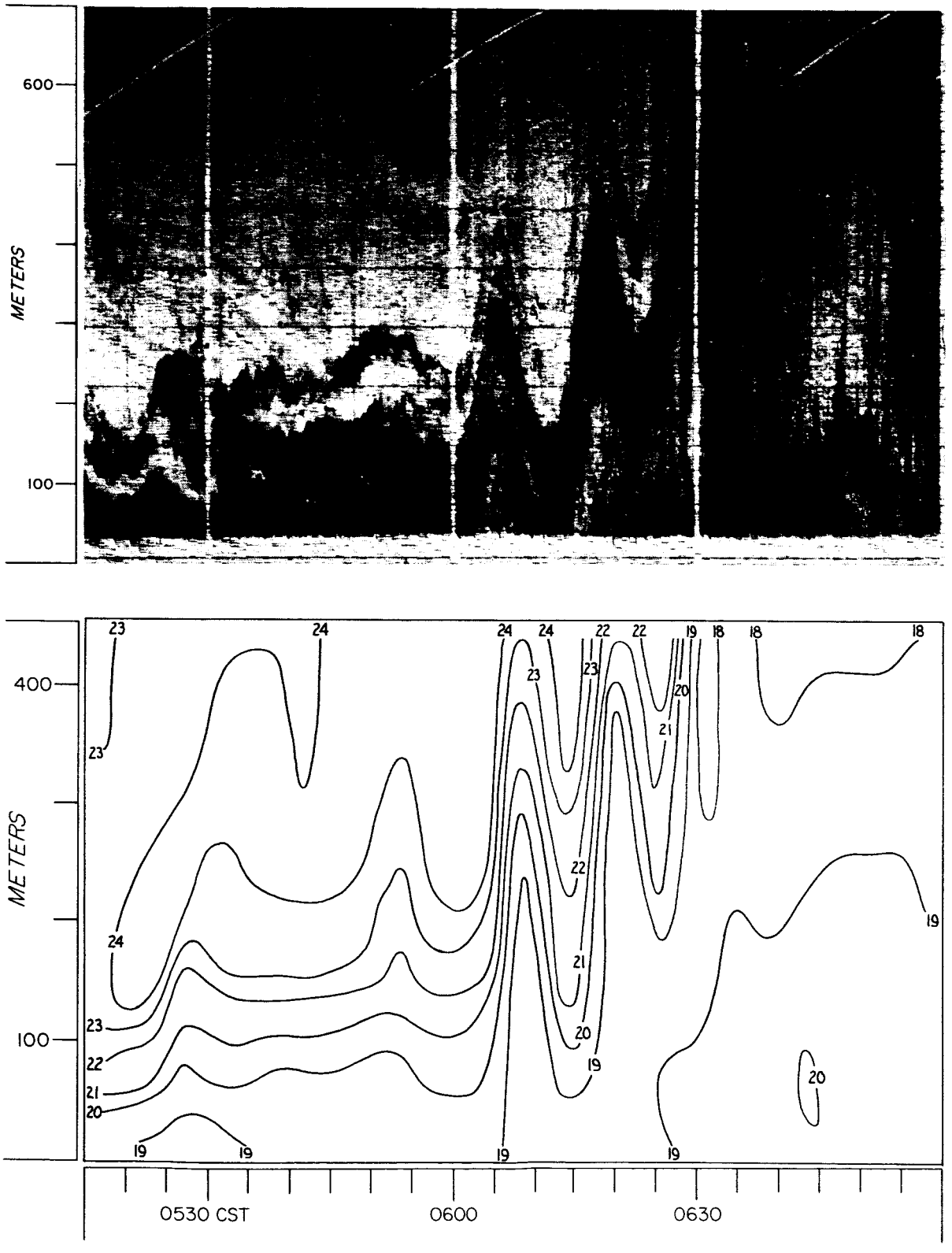

Fig. 12. Acoustic radar facsimile record (a) and time section of temperature (degrees C) (b) for 0515-0700 CST 9 August 1972.

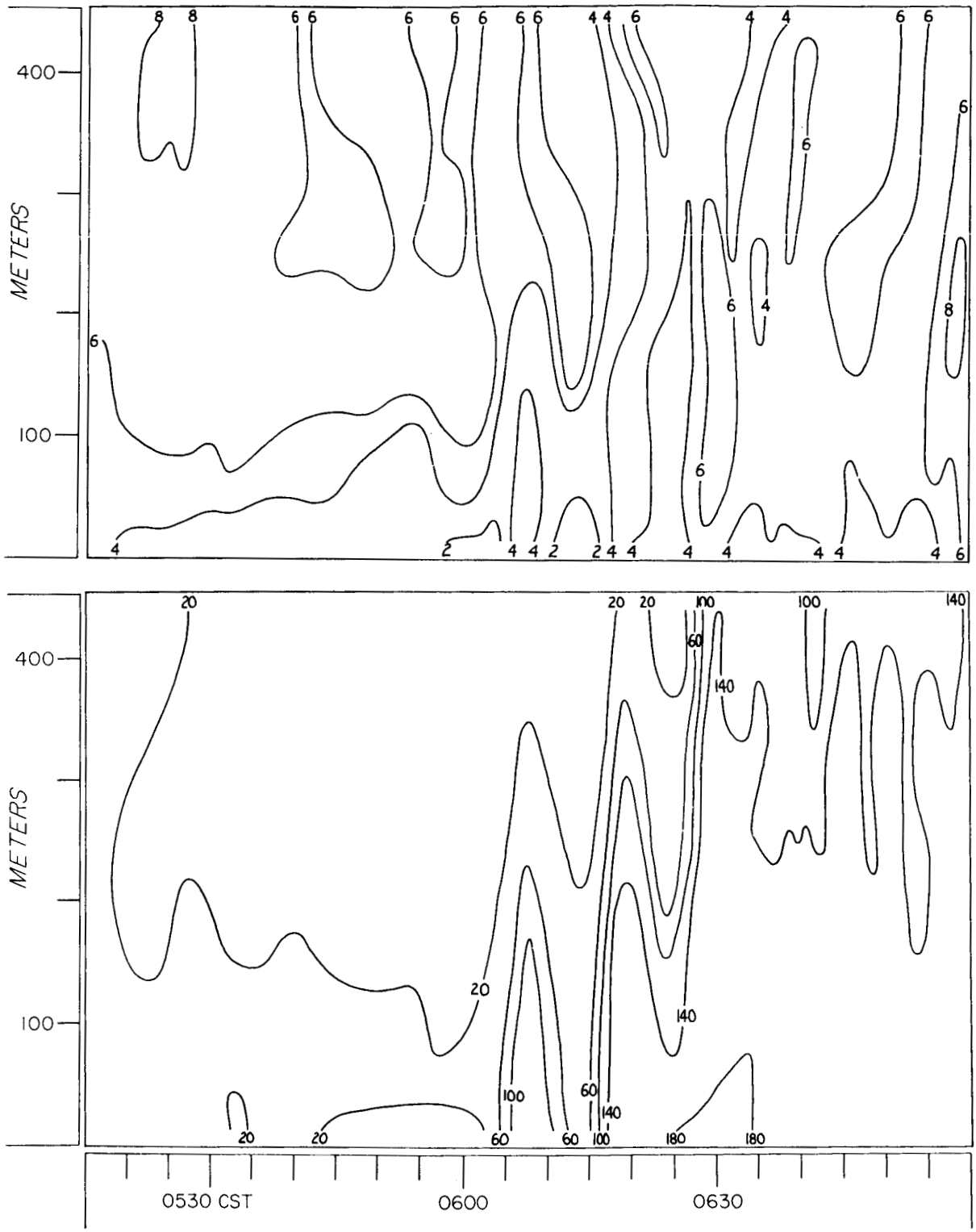

Fig. 12. Time section of wind speed ($msec^{-1}$) (c) and wind direction (degrees) (d) for 0515-0700 CST 9 August 1972.

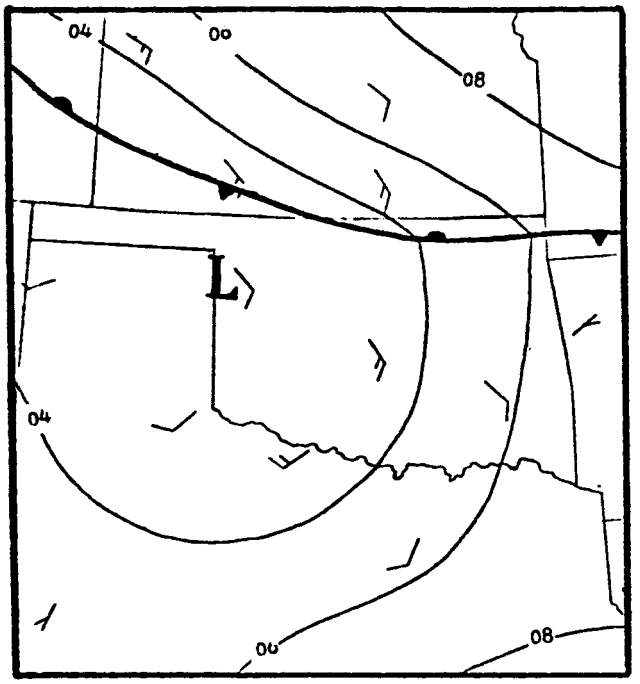

Fig. 13a. Surface analysis for 0000 CST 26 June 1972 (pressure contours in millibars, i.e., 08 = 1008 mb).

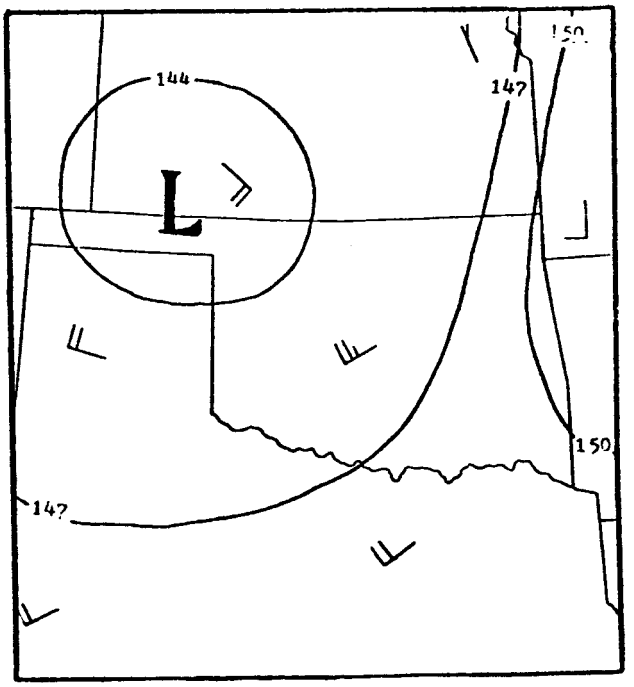

Fig. 13b. Height contour patterns at the 850 mb level for 0600 CST 26 June 1972 (contour interval is 30 m).

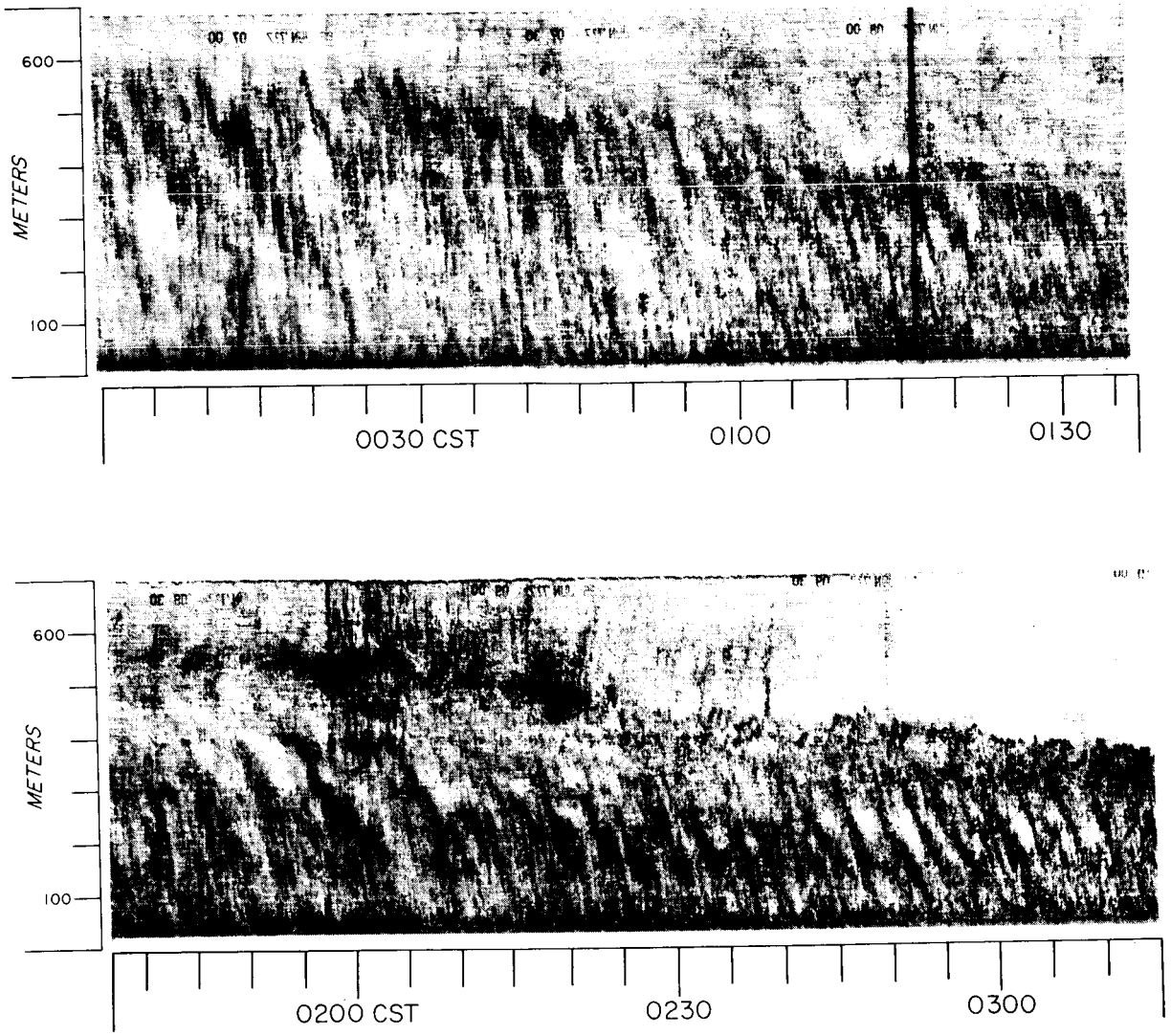

Fig. 14. Acoustic radar facsimile record for 0000-0137 CST (a) and acoustic radar facsimile record for 0138-0315 CST (b) 26 June 1972.

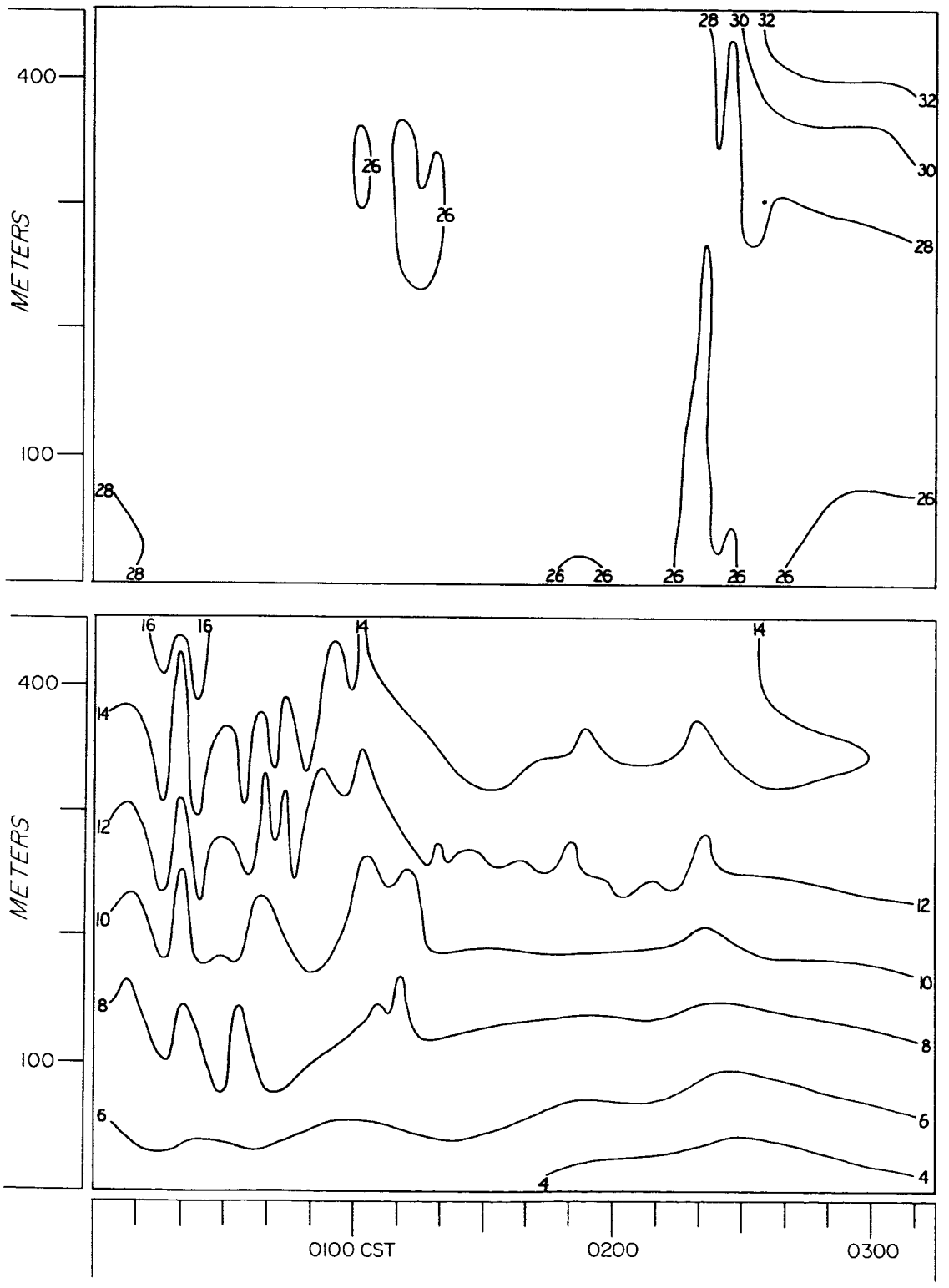

Fig. 14. Time section of temperature (Degrees C) (c) and time section of wind speed ($msec^{-1}$) (d) for 0000-0315 CST 26 June 1972.

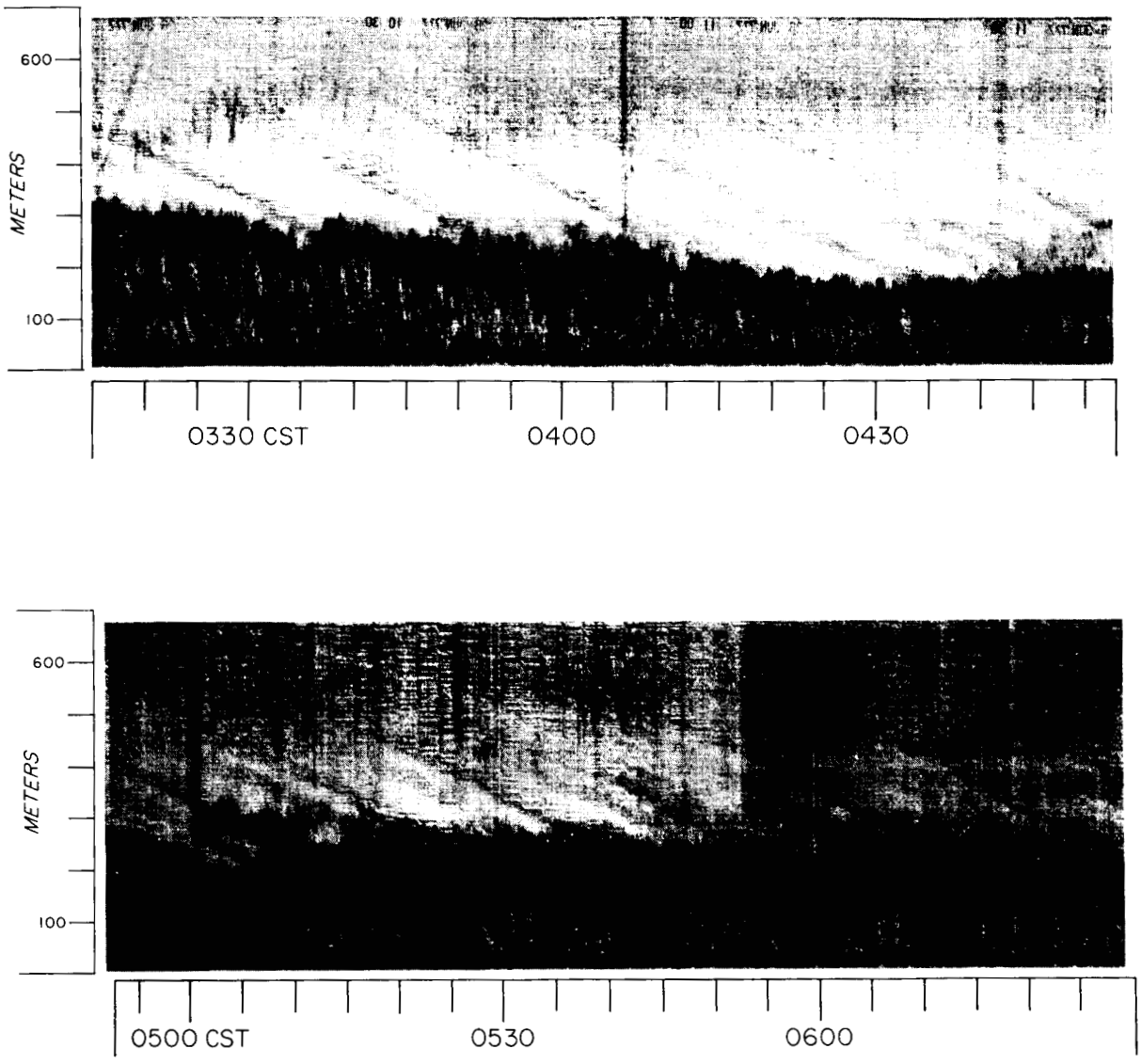

Fig. 15. Acoustic radar facsimile record for 0315-0452 CST (a) and acoustic radar facsimile record for 0452-0630 CST (b) 26 June 1972.

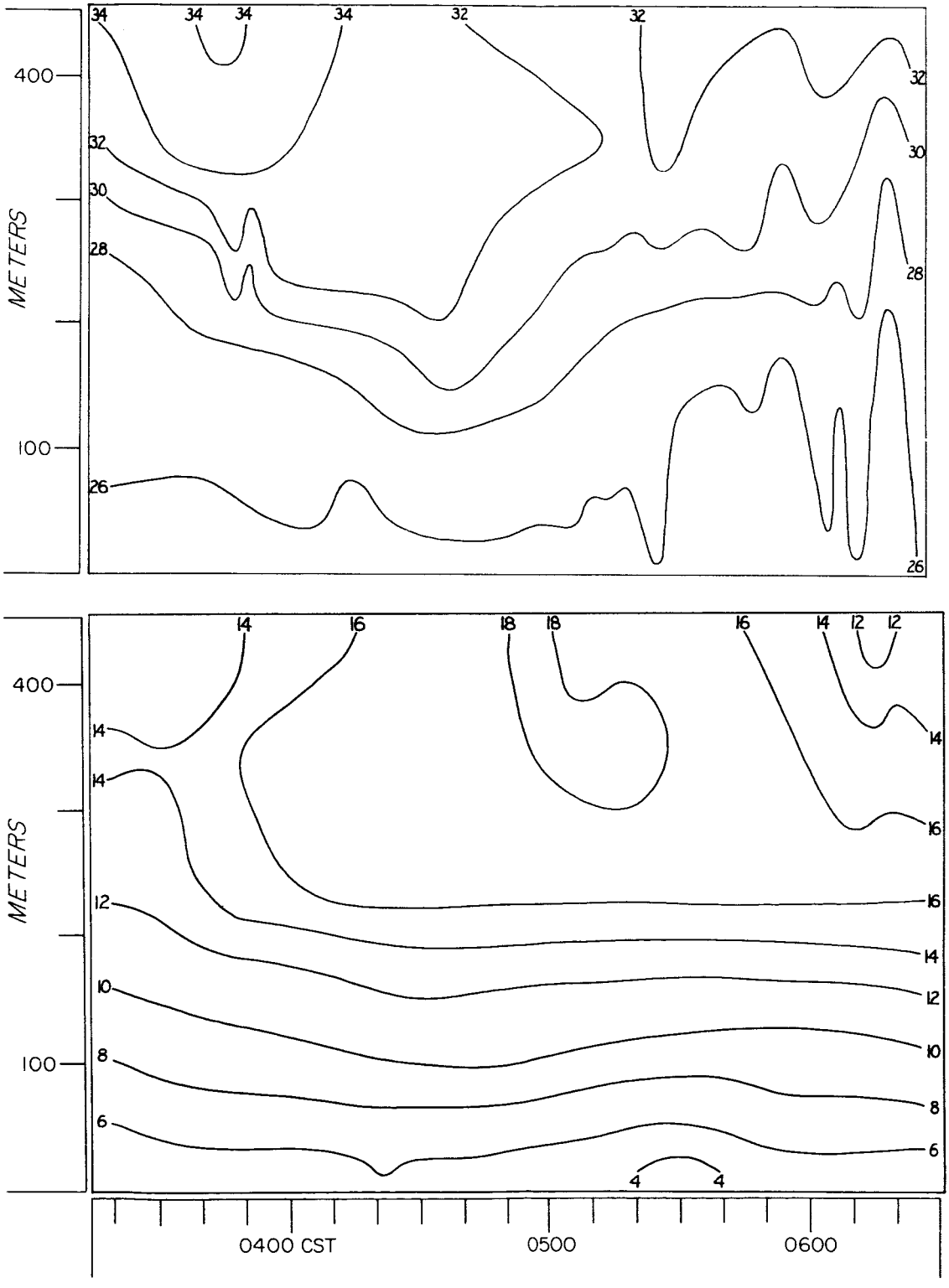

Fig. 15. Time section of temperature (degrees C) (c) and time section of wind speed ($msec^{-1}$) (d) for 0315-0630 CST 26 June 1972.

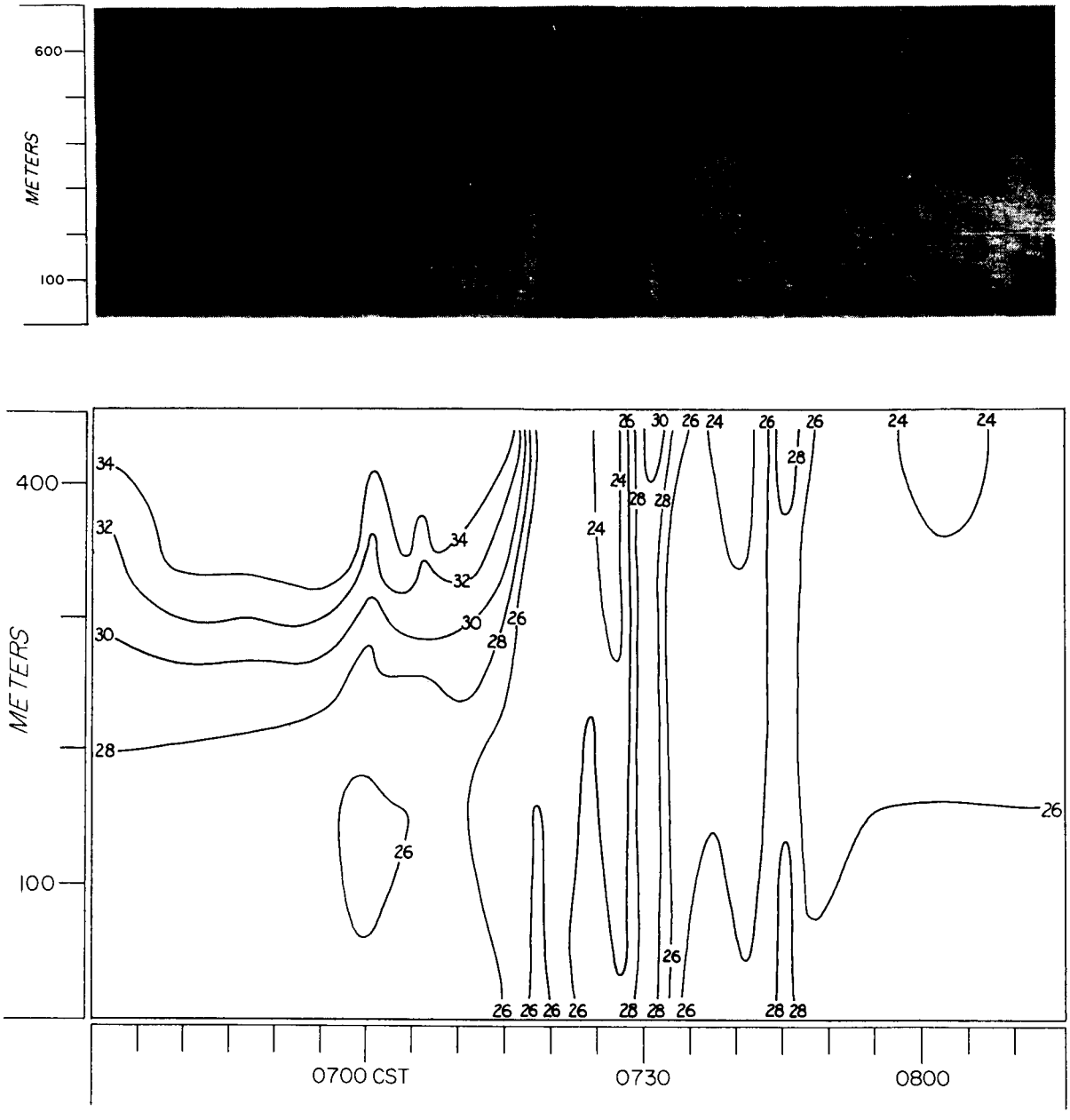

Fig. 16. Acoustic radar facsimile record (a) and time section of temperature (degrees C) (b) for 0630-0815 CST 26 June 1972.

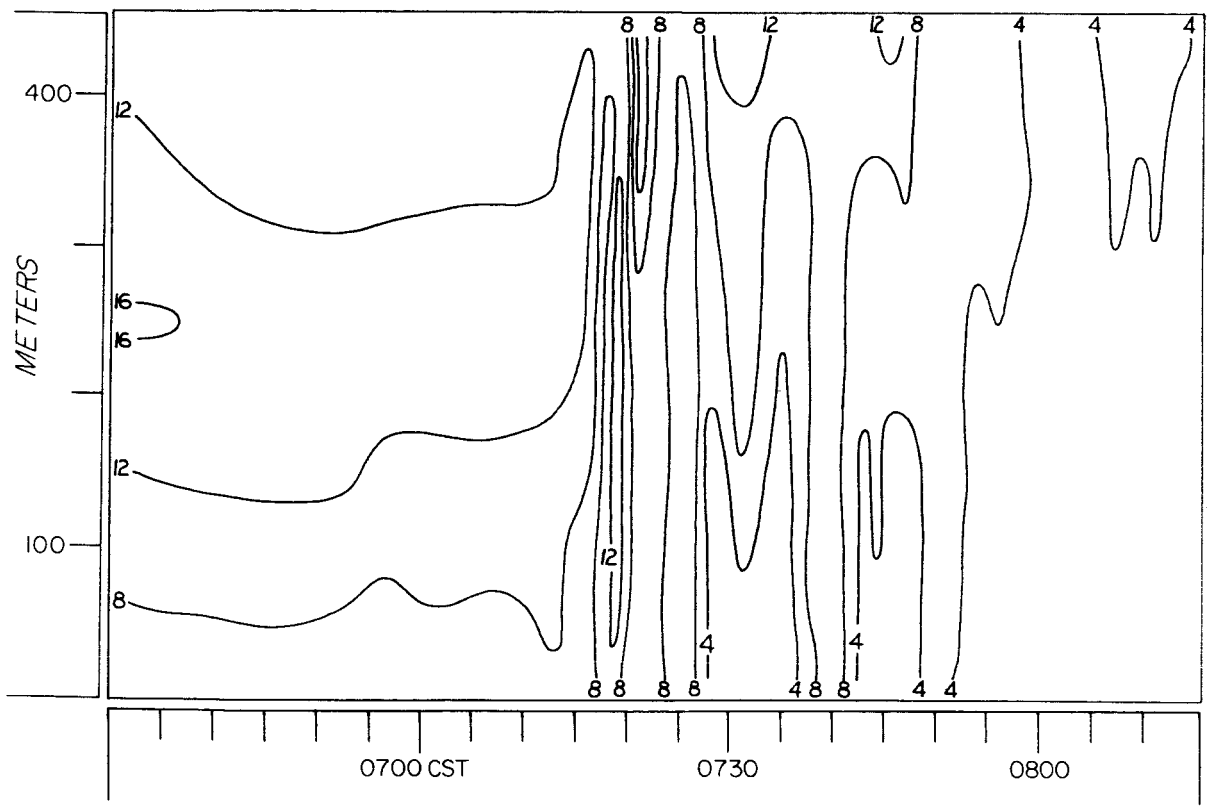

Fig. 16. Time section of wind speed ($msec^{-1}$) (c) for 0630-0815 CST 26 June 1972.

NASA-Langley, 1974